Research Square

Preprints are preliminary reports that have not undergone peer review.
They should not be considered conclusive, used to inform clinical practice,
or referenced by the media as validated information.

The SHP-2/ZEB1-Centered Network Promotes Breast Cancer Cell Migration and Invasion through a Multi-Step and Homeostatic Mechanism

Bin Lei
Southwest Medical University
Meiping Yan
ymp1989@swmu.edu.cn
Southwest Medical University

Research Article

Keywords: breast cancer, SHP-2, dimers, disulfide bonds, phosphatase activity

Posted Date: November 23rd, 2026

DOI: https://doi.org/10.21203/rs.3.rs-11347615/v1

License: This work is licensed under a Creative Commons Attribution 4.0 International License.
Read Full License

Additional Declarations: No competing interests reported.

The SHP-2/ZEB1-Centered Network Promotes Breast Cancer Cell Migration and Invasion through a Multi-Step and Homeostatic Mechanism

Bin Lei, Meiping Yan*

The Research Center for Preclinical Medicine, Southwest Medical University, Luzhou, Sichuan, China 646000.
Correspondence to:
Meiping Yan, e-mail: ymp1989@swmu.edu.cn.

Abstract

Background SHP-2 is a tyrosine phosphatase that can both promote and inhibit cancer progression. Its expression varies in breast cancer, and its precise role remains unclear.

Methods Immunohistochemistry and Western blot analyses of breast cancer samples and representative cell lines further validated the expression discrepancy. Phosphorylation of SHP-2 was then selected as the candidate affecting its expression after excluding genetic variation and alternative splicing via Sanger sequencing, phosphatase assays, and RT-qPCR. ZEB1 was identified as a key downstream target dynamically regulated by SHP-2 and involved in a positive feedback regulation of SHP-2 phosphorylation, demonstrated by SHP-2 overexpression, knockdown, and knockout experiments. Subsequently, transcriptome sequencing, cytokine arrays, and so on were performed to elucidate the downstream effects of ZEB1. SHP-2 dimerization was analyzed using site-directed mutagenesis, SEC-MALS, diagonal electrophoresis, mass spectrometry. Finally, several stimuli were selected to analyze the dynamic regulation of SHP-2-mediated pathways.

Results We found that SHP-2 is expressed at lower levels but is highly phosphorylated at Y542 and Y580 in certain cell lines. This discrepancy results from the interplay between the SHP-2/ZEB1 positive feedback loop and negative regulatory pathways. This loop promotes breast cancer cell migration and invasion by activating PI3K/AKT, MEK/ERK, SRC/YAP1, and STAT3 signaling. SHP-2 dynamically modulates parafibromin to initially inhibit, then subsequently increase ZEB1 expression, which upregulates gp130 and activates SHP-2 via IL-6 signaling. Notably, SHP-2 promotes ZEB1 in BT-549 cells but inhibits it in T-47D cells. We also found that SHP-2 predominantly exists as dimers stabilized by disulfide bonds, secondary interactions, and other post-translational modifications (PTMs), which explains its variable roles across different cell types and time points. Therefore, SHP-2's effect on breast cancer depends on its conformational state, with phosphatase activity directly regulated by disulfide bonds. Phosphorylation by EPHA2 correlates with increased phosphatase activity and protein degradation and can be enhanced by various stimuli.

Conclusions We identified a SHP-2/ZEB1-centered network that contributes to the discrepancies of SHP-2 in breast cancer. SHP-2 primarily exists as dimers, with its structure and function regulated by disulfide bonds, secondary interactions, and other PTMs. These findings explain why PTPN11 can act as both an oncogene and tumor suppressor. Finally, we propose that the SHP-2 complex mediates signal transduction via a multi-step, balanced mechanism.

Key words breast cancer; SHP-2; dimers; disulfide bonds; phosphatase activity

Introduction

Breast cancer, one of the most commonly diagnosed cancers worldwide (International Agency for Research on Cancer), is biologically heterogeneous, exhibiting variation in pathology, gene expression, genomic alterations, and the tumor microenvironment [1]. Although patient survival has improved due to advances in surgery, mammographic screening, and adjuvant therapies [2], mortality remains high in triple-negative breast cancer (TNBC). Therefore, understanding the mechanisms driving TNBC invasiveness and identifying effective drug targets is essential.

Signal transduction is crucial for cellular processes such as proliferation, differentiation, and inflammation [3]. Protein tyrosine phosphorylation and dephosphorylation, regulated by protein tyrosine kinases (PTKs) and protein tyrosine phosphatases (PTPs), play a critical role in intracellular signaling [4]. Dysregulation of these enzymes contributes to cancer development and metastasis. SHP-2, the first identified cancer-promoting PTP, has attracted significant attention [5]. Encoded by the *PTPN11* gene, SHP-2 is highly conserved and comprises two Src homology 2 (SH2) domains, a PTP domain, and a C-terminal tail [6]. Its function as either an oncogene or a tumor suppressor remains controversial. SHP-2 suppresses hepatocellular carcinogenesis by downregulating inflammatory signaling [7], yet it promotes breast cancer progression by activating multiple signaling pathways [8-10]. However, an immunohistochemical analysis of 1,401 breast cancer specimens revealed that only 651 (46%) were SHP-2 positive [11].

This study investigates the causes of discrepancies in SHP-2 expression and its role in breast cancer. The SHP-2/ZEB1 positive feedback loop is a key regulator of cell migration and invasion, modulated by several negative feedback mechanisms. This regulatory network contributes to the variability of SHP-2 expression. Additionally, SHP-2 forms dimers through disulfide bonds and secondary interactions, with its phosphatase activity directly regulated by disulfide bonds, particularly those involving C459 and other cysteine residues. Phosphorylation at Y542 and Y580 positively correlates with phosphatase activity and protein degradation. Various stimuli can increase SHP-2 phosphorylation. Finally, we propose a multi-step, balanced signal transduction model for SHP-2.

Materials and methods

Reagents and antibodies

Reagents: Cycloheximide (HY-12320), recombinant human EGF (HY-P7109), IL-6 (HY-P7044A), IL-8/CXCL8 (HY-P7224), PDGF-AA (HY-P70598), IL6Rα (HY-P70515), ML-099 (HY-124306), PD98059 (HY-12028), LY294002 (HY-10108), Actinomycin D (HY-17559), protease inhibitor cocktail (HY-K0010), and protein A/G magnetic beads (HY-K0202) were from MedChemExpress (New Jersey, USA). Puromycin dihydrochloride (T2219), MG132 (T2154), Rapamycin (T1537), and Napabucasin (T3218) were from TargetMol (Boston, USA). Phosphatase inhibitor cocktail (PR20015) was from Proteintech (Wuhan, China). Recombinant human TGF-β1 (91701ES08) and Matrigel matrix (40183ES10) were from Yeasen (Shanghai, China). DiFMUP (11627) was from AAT Bioquest (Pleasanton, USA). DL-Dithiothreitol (D104859), N-Ethylmaleimide (E100553), and reduced glutathione (G105426) were from Aladdin (Shanghai, China). 3% Hydrogen Peroxide (029161) was from HuanKai Microbial (Guangzhou, China). Total RNA Kit, Gel Extraction Kit, and Endo-free Plasmid Mini Kit were from Omega Bio-Tek (Norcross, USA). All-In-One 5×RT MasterMix and BlasTaq 2×qPCR MasterMix were from Applied Biological Materials (Richmond, Canada). PrimeScript II 1st Strand cDNA Synthesis Kit, PrimeSTAR GXL DNA Polymerase, T4 ligase, and restriction endonucleases were from Takara (Kyoto, Japan). Dual-Luciferase Reporter

Assay System, Hieff NGS Ultima Dual-mode mRNA Library Prep Kit, Hieff NGS In-Situ DNA Binding Profiling Library Prep Kit for Illumina, Hieff NGS Tagment Index Kit, dsDNA HS Assay kit, and growth factor reduced Matrigel were from Yeasen (Shanghai, China). Human Cytokine Antibody Array C5 was from RayBiotech (Pichitrakonas, USA). IL-6 (RK00004) and IL-8 (RK00011) ELISA kits and Dpn1 enzyme were from Abclonal (Wuhan, China). ER protein isolation kit was from BestBio (Shanghai, China). MDA-MB-468, MDA-MB-361, HCC-1954, and UACC-812 cell lines were from Pricella (Wuhan, China); SKBR-3 was from Servicebio Technology (Wuhan, China). Dulbecco's modified Eagle's medium was from Thermo Fisher Scientific (Waltham, USA). Related plasmids were from Miaoling Biotechnology (Wuhan, China). DH5α and pClone007 Versatile Simple Vector Kit were from Tsingke Biotech (Beijing, China). Human breast cancer tissue chips were from Shanghai Outdo Biotech (Shanghai, China). Phos-tag Acrylamide and infrared-labeled or unlabeled DNA probes were synthesized by Viagene Biotech (Changzhou, China). SiRNAs were from GenePharma (Shanghai, China) and General Biol (Chuzhou, China). Sequences are listed in Supplementary Table 1.

Antibody: Antibodies against SHP-2 (20145-1-AP), YAP1 (13584-1-AP), TAZ (23306-1-AP), ZEB1 (21544-1-AP), ZEB2 (14026-1-AP), AKT (10176-2-AP), β-Catenin (51067-2-AP), IL-6Rα (23457-1-AP), phospho-ERK1/2 (T202/Y204, 28733-1-AP), ZO-1 (21773-1-AP), JUN (24909-1-AP), ETS1 (12118-1-AP), GSK3B (22104-1-AP), phospho-GSK3B (Ser9, 67558-1-Ig), Vimentin (10366-1-AP), GAPDH (10494-1-AP), FLAG (20543-1-AP), and HA (51064-2-AP) were purchased from Proteintech (Wuhan, China). Antibodies against EPHA2 (A23177), gp130 (A14656), phospho-EPHA2 Y772 (AP0817), phospho-EPHA2 S897 (AP1082), phospho-AKT (Ser473, AP1453), Src (A19119), and P4HB (A19239) were from Abclonal (Wuhan, China). EGFR (4267), phospho-EGFR (Y1068, 3777), Stat3 (30835S), phospho-Stat3 (Y705, 9131S), histone H3 (4620S), phospho-SHP-2 (Y580, 5431) and p44/42 MAPK (Erk1/2, 4695), and secondary anti-rabbit (7074) and anti-mouse (7076) antibodies were obtained from Cell Signaling Technology (Danvers, USA). SHP-2 (B-1, sc-7384) antibody was from Santa Cruz Biotechnology (Santa Cruz, USA). JAK1 (BS1193) antibodies were from Bioworld Technology (MN, USA). Phospho-Src (Y419, BM4307) antibody was from BOSTER Biological Technology (Wuhan, China). Calreticulin (F0472), mTOR (F0169), phospho-mTOR (Ser2448, F2584), and c-Myc/N-Myc (F2664) antibodies were obtained from Selleck (Houston, USA).

Cell culture and transfection

Cell lines MDA-MB-231, MDA-MB-468, MDA-MB-361, T-47D, T-47D PTPN11$^{-/-}$, MCF-7, and HeLa were cultured in Dulbecco's Modified Eagle's Medium (DMEM). BT-549 and HCC-1954 were grown in RPMI 1640, with BT-549 PTPN11$^{-/-}$ supplemented with 10 μM ML-099. UACC-812 was cultured in Leibovitz's L-15 medium, SKBR-3 in McCoy's 5A, and MCF-10A in DMEM/F12 supplemented with 5% horse serum, 20 ng/mL EGF, 0.5 μg/mL hydrocortisone, 10 μg/mL insulin, and 1% non-essential amino acids. All media contained 10% fetal bovine serum (FBS), 100 U/mL penicillin, and 100 μg/mL streptomycin, except MDA-MB-361, which was maintained in DMEM with 20% FBS. Cells were cultured at 37°C with 5% CO2, tested for mycoplasma contamination, and transfected according to the manufacturer's protocol.

Generation of stable cell lines via lentiviral infection

Lentiviruses expressing FLAG-PTPN11 or PTPN11 shRNA were produced by Generalbiol. The shRNA target sequences are: 5'-TGGAGATGTCATTGAGCTTAA-3', 5'-ATGCGTGTTAGGAACGTCAAA-3', and 5'-CAGAAGCACAGTACCGATTTA-3'. T-47D,

MDA-MB-231, MDA-MB-468, and MDA-MB-361 cell lines were infected with these lentiviruses at various MOIs in medium supplemented with 5 μg/mL polybrene. After 2 days, cells were selected with 0.5 μg/mL puromycin for 7 days before mRNA or protein extraction.

Generation of *PTPN11* knockout cell lines

PTPN11 knockout breast cancer cell lines were created using CRISPR/Cas9 gene editing. The gRNA (gRNA-A1: GAGACTTCACACTTTCCGTTAGG) targeted the coding region on exon 2 [9]. gRNA and Cas9 protein were co-transfected into BT-549 and T-47D cells via electroporation. Single colonies were isolated and confirmed by Sanger sequencing and Western blot.

RNA extraction and Real-time qPCR

Total RNA was extracted using a Total RNA Kit, and reverse transcription was performed with 5× RT MasterMix following the product manuals. Real-time quantitative PCR was conducted with BlasTaq 2× qPCR MasterMix on a CFX-96 system. Gene expression levels were calculated using the 2^-ΔΔCt method. Primers were designed using Primer Premier 5 or PrimerBank [12], with sequences provided in Supplementary Table 2.

Plasmid construction

Plasmid templates were derived from BT-549 cells. Total RNA was extracted using a Total RNA Kit or phenol-chloroform method, followed by reverse transcription PCR with the PrimeScript II 1st Strand cDNA Synthesis Kit to obtain full-length cDNA. The template was amplified using PrimeSTAR GXL DNA Polymerase. PCR products were purified with a Gel Extraction Kit and ligated into expression vectors via double digestion and T4 ligation. DNA templates were extracted from cells by phenol-chloroform extraction, and promoter fragments were amplified using PrimeSTAR GXL DNA Polymerase. Fragments were digested with restriction enzymes and ligated into the pGL3 vector. Recombinant plasmids were transformed into DH5α, and positive clones were selected for sequencing. Mutant and splicing isoform plasmids were generated by DpnI digestion or fusion PCR. All plasmids were confirmed by Sanger sequencing and extracted using an endotoxin-free plasmid mini kit.

Luciferase reporter assays

BT-549 or HeLa cells were co-transfected with the indicated pGL3 basic vector, luciferase reporter plasmid, pRL-TK plasmid, YAP1, ETS1, JUN, and ZEB1 expression plasmid. Equal DNA amounts were used for test and control groups. After transfection, cells were lysed using the assay kit buffer. Luciferase activities were measured following the Dual-Luciferase Reporter Assay System protocol. Firefly luciferase activity was normalized to *Renilla* luciferase activity.

Breast cancer cell-conditioned media

Breast cancer cell lines BT-549, MDA-MB-231, T-47D, and MDA-MB-361 were grown to 90% confluence in 100-mm dishes. After rinsing twice with preheated basal medium, cells were cultured for 24 hours in 1% FBS 1640 or DMEM. The conditioned media were centrifuged at 4°C to remove cells and then ultrafiltered using 3 kDa Ultra 15 mL filter devices.

Cytokine antibody assay

The secreted cytokine protein levels in ultrafiltered conditioned media were measured using the Human Cytokine Antibody Array C5, following the manufacturer's instructions. Cytokine array membranes were blocked for 30 minutes at room temperature, then incubated overnight at 4°C with conditioned media. After four washes, membranes were incubated with a biotinylated antibody cocktail and HRP-streptavidin. Chemiluminescence images were then captured and analyzed using the G:BOX Chemi Imager.

ELISA

IL-6 and IL-8 levels in cell culture supernatants were measured using human ELISA kits following the manufacturer's instructions. Absorbance was read at 450 nm with a Multi-scan GO Microplate Reader.

Isolation of endoplasmic reticulum (ER) proteins

The ER protein isolation kit was used for ER protein detection and analysis. Two 100 mm dishes of cells at 90% confluence were harvested, washed twice with cold PBS, and lysed in 500 μL of solution A on ice for 10 minutes. Cells were homogenized using a Dounce homogenizer. After three centrifugations at varying speeds, the supernatant was transferred to a new tube. Then, 125 μL of solution B was added, mixed thoroughly, and the sample was incubated at 4°C overnight. It was centrifuged at 10,000 × g for 45 minutes at 4°C, and the pellet was resuspended in 100 μL of solution C.

Cytoplasmic and nuclear protein extraction procedures

After 48 hours of transfection, BT-549 cells were harvested. Cytoplasmic proteins were extracted using a hypotonic buffer, while nuclear proteins were obtained by lysing the pellet in a hypertonic buffer following high-speed centrifugation.

Immunoprecipitation (IP)

Cells were lysed in NP-40 buffer with protease inhibitors. After high-speed centrifugation, the supernatant was incubated overnight at 4°C with 1 μg antibody and constant rotation. Then, 20 μL protein A/G magnetic beads were added and incubated for 1 hour at 4°C with rotation. Beads were washed at least four times with NP-40 buffer, then proteins were eluted in lysis buffer with SDS loading buffer after heating at 100°C for 10 minutes. For the phosphate activity assay, beads were washed twice with lysis buffer and twice with reaction buffer without protease inhibitors. Beads were then suspended in 250 μL reaction buffer containing 20 nM DiFMUP and incubated at 37°C for 30 minutes. Phosphate activity was measured using a SpectraMax i3x microplate reader.

Western Blot analysis

Confluent cells in 60-mm dishes were washed with PBS and lysed in RIPA buffer (150 mM NaCl, 50 mM Tris-HCl pH 7.6, 10 mM MgCl2, 1% Triton X-100, 0.25% deoxycholic acid, 0.1% SDS) containing protease and phosphatase inhibitors. After 30 minutes on ice, lysates were centrifuged at 12,000 rpm and 4°C for 20 minutes. Supernatants were mixed with SDS loading buffer and boiled for 10 minutes. Samples were separated on 7.5% SDS-PAGE gels and transferred to 0.2 μm PVDF membranes. Membranes were blocked for 1 hour at room temperature in 5% fat-free milk, then incubated overnight at 4°C with primary antibodies. After three washes with TBST, membranes were incubated with secondary antibodies for 1 hour at room temperature, followed by four TBST washes. Images were captured and analyzed using a G:BOX Chemi Imager.

Denaturing non-reducing electrophoresis

The procedure was the same as Western Blot analysis, except the non-reducing sample lacked a reducing agent. Additionally, the non-reducing sample volume was generally twice that of the reducing sample.

Native PAGE

Cells were lysed in NP-40 buffer with protease inhibitors. Supernatants were mixed with native PAGE loading buffer and separated on 4-16% bis-tris CN-PAGE gels per the manufacturer’s instructions. Proteins were transferred to PVDF membranes, blocked, and incubated with primary and secondary antibodies.

Sequential non-reducing/reducing two-dimensional SDS-PAGE or diagonal electrophoresis

Confluent cells in 100-mm dishes were harvested, lysed with lysis buffer, and denatured either at 100°C for 10 minutes or 37°C for 1 hour without reducing agents. Samples were first separated under nonreducing conditions on 7.5% PAGE gels using SDS running buffer. To reduce disulfide bonds, lanes were incubated at 65°C with 250 mM DTT in SDS buffer for 25 minutes, then washed and incubated with 100 mM NEM for 25 minutes at room temperature. Control samples were incubated in SDS buffer under the same temperature conditions. Gentle shaking was applied throughout. After second-dimension electrophoresis, gels underwent immunoblotting [13].

Phos-tag SDS-PAGE

Phos-tag SDS-PAGE was performed following the Phos-tag Acrylamide user manual. Whole cell extracts were run on phosphate affinity SDS-PAGE gels containing Phos-tag with Mn^{2+}. Standard stacking (4.5% acrylamide) and separating gels (7.5% acrylamide, 50 μM Phos-tag, 100 μM $MnCl_2$) were used. Electrophoresis was conducted at 75 V for 30 minutes, then 150 V until the dye front reached the gel bottom, on ice. Before transfer to PVDF membranes, gels were washed three times for 30 minutes each in transfer buffer with 10 mM EDTA, followed by a 20-minute wash in transfer buffer without EDTA [14].

Immunohistochemical staining

After blocking with 10% goat serum for 30 minutes at room temperature, tissue sections were incubated overnight at 4°C with SHP-2 antibody (1:200, 20145-1-AP). They were then incubated with HRP-linked goat anti-rabbit secondary antibody for 1 hour at 37°C and stained using a DAB kit. Images were scanned with a KF-PRO-002 digital pathology slide scanner (KONFOONG Bioinformation Tech, China) and analyzed using ImageJ software.

Cell migration and invasion assays

Cell migration assays were conducted using Transwell inserts (8-μm pores, Falcon). A total of 1 × 10^4 cells in 100 μL medium with 1% FBS were placed in the upper chamber, while 600 μL medium containing 10% FBS was added to the lower chamber. After 24 hours, migrated cells were fixed, stained with crystal violet, and imaged under a phase-contrast microscope. For invasion assays, the upper side of the Transwell inserts was precoated with growth factor-reduced Matrigel diluted 1:8 in cold, serum-free medium and incubated for 3-4 hours to allow gel formation. Subsequent steps were identical to the migration assay.

Chromatin immunoprecipitation (ChIP) assay

ChIP assay was performed using the fast chromatin immunoprecipitation method [15]. Cells were cross-linked with 1% formaldehyde, harvested, and sonicated using a Bioruptor Pico following standard protocols. The supernatant was collected for immunoprecipitation (IP), and the resulting samples were used for DNA isolation. The isolated DNA was then analyzed by PCR.

EMSA

BT-549 cells were cultured overnight in 1% FBS 1640 medium, then stimulated with 50 ng/mL IL-6 and 20 ng/mL EGF for 12 hours. Nuclear proteins were isolated from scraped cells. Binding reactions were conducted by incubating nuclear extracts with IR-labeled or unlabeled probes for 30 minutes at room temperature, following the IR DNA-EMSA kit protocol. Fluorescence detection was performed using Li-Cor Odyssey infrared scanners.

Sanger sequencing

DNA and RNA were extracted from various cell lines. Full-length cDNA was synthesized using the PrimeScript II 1st Strand cDNA Synthesis Kit via reverse transcription PCR. Sequences were

amplified with PrimeSTAR GXL DNA Polymerase, then cloned into vectors using the pClone007 Versatile Simple Vector Kit. Plasmids were transformed into DH5α, and at least two positive clones were selected for sequencing. Alternatively, PCR products were purified with a Gel Extraction Kit and directly sent for Sanger sequencing.

Transcriptome sequencing

The Hieff NGS Ultima Dual-mode mRNA Library Prep Kit was used to construct transcriptome libraries following the manufacturer's instructions. Total RNA was isolated from BT-549, T-47D, MDA-MB-231, and MDA-MB-361 cells. mRNA purification and fragmentation were performed using mRNA capture beads and high-temperature interruption. First-strand cDNA synthesis was carried out with the 1st strand enzyme mix, followed by second-strand synthesis, complementation, and A-tail addition using the 2nd strand enzyme mix. Adapter ligation and fragment purification were then performed. Library amplification was achieved via PCR using Hieff NGS 384 CDI Primer for Illumina. DNA Selection Beads purified the library, which was quantified with the dsDNA HS Assay kit before sequencing on an Illumina NovaSeq 150PE.

Cleavage Under Targets and Tagmentation Sequencing (CUT&Tag sequencing)

The Hieff NGS In-Situ DNA Binding Profiling Library Prep Kit for Illumina was used according to the manufacturer's instructions. BT-549 cells were bound to concanavalin A-coated beads, then resuspended in antibody buffer and sequentially treated with primary and secondary antibodies against ZEB1. Samples were incubated with pA/G-Tn5 transposase simultaneously. After transposon activation and tagmentation, DNA was isolated and purified. Libraries were constructed using the Hieff NGS Tagment Index Kit for Illumina and PCR amplification [16, 17], then purified with DNA Selection Beads. Library quantification was performed using the dsDNA HS Assay kit before sequencing on an Illumina NovaSeq 150PE.

Purification of recombinant human SHP-2 from HEK293 cells

A cDNA encoding full-length human SHP-2 was cloned into the pGSHC vector and expressed as a fusion protein with an N-terminal signal peptide and a C-terminal 6×His tag in mammalian HEK-293 suspension cells. Cells were cultured at 37°C with shaking at 130 rpm for 6 days. The culture supernatant was collected, centrifuged, and filtered through a 0.22 μm membrane. The target protein was purified using Protein A resin. Purified SHP-2 was analyzed by SDS-PAGE with Coomassie Brilliant Blue staining and immunoblotting using an anti-SHP-2 antibody.

Size exclusion chromatography-multi-angle light scattering (SEC-MALS)

Size-exclusion chromatography (SEC) was performed using a Waters gel permeation system. The SHP-2 protein solution was filtered through a 0.22 μm membrane, and the supernatant was loaded into a 250 μL inner column. A 50 μL sample was injected at 1 mL/min with a mobile phase of 0.1 M NaNO3 aqueous solution. The column temperature was maintained at 30°C. The SEC system was equipped with a multi-angle light scattering (MALS) detector at 15° and 90° angles, along with a refractive index (RI) detector.

Mass spectrometry (MS)

The IP samples were loaded onto a 7.5% SDS-PAGE gel and stained with Rapid Protein Stain solution. The gel-embedded protein samples were then analyzed by LC-MS/MS, with data analysis conducted by the company. After reduction and alkylation, the samples underwent trypsin digestion for 20 hours. Peptides were separated using a nanoElute system and analyzed by a tims-TOF Pro mass spectrometer for 30 minutes.

Disulfide bond mass spectrometry analysis

An appropriate amount of purified protein was treated with guanidine hydrochloride and iodoacetamide at 37°C to denature and block free cysteines. The sample was then exchanged with Tris-HCl solution, followed by additional iodoacetamide to prevent disulfide bond mismatches. Trypsin digestion was performed overnight. After digestion, the sample was desalted using a C18 Tip column, freeze-dried, and reconstituted in 0.1% formic acid. The peptides were separated by nanoliter high-performance liquid chromatography and analyzed by high-resolution mass spectrometry using HCD fragmentation. The mass spectrometry using HCD fragmentation. Data were processed with pLink software. Reason: The revision improves clarity, flow, and technical accuracy by breaking complex sentences into concise steps and correcting grammar. The shortened version retains essential procedural details while eliminating redundancies for brevity.

Statistical analysis

Cell counting and protein band intensity were measured using ImageJ (v2.9.0). Statistical analyses were conducted with GraphPad Prism (v6.0). Data are presented as mean ± standard deviation (SD). Group comparisons employed unpaired two-tailed Student's *t*-test, one-way ANOVA, or two-way ANOVA with Bonferroni's multiple comparisons test. Significance is denoted by asterisks: *P<0.05; **P<0.01; ***P<0.001, with P<0.05 considered significant. Biological sequences were illustrated using IBS 1.0. Sequencing results were aligned to the human reference genome via Hisat2, and analyzed with DESeq2R. Biological process pathway analysis was performed using Gene Ontology (GO).

Results

SHP-2 is Expressed at Low Levels but undergoes Highly Tyrosine Phosphorylation in Certain Cell Lines

As previously reported, SHP-2 expression varies in breast cancer (Fig. 1A, 1B, S1A). The more invasive subtypes, BT-549 and MDA-MB-468, show relatively low SHP-2 levels (Fig. 1C, 1D, S1B). However, SHP-2 enhances cell migration and invasion in a phosphatase-dependent manner (Fig. 1E). Overexpression of SHP-2 increases Vimentin and decreases Zonula Occludens-1 (ZO-1) levels (Fig. 1F). Although these findings may appear contradictory, we propose that SHP-2 in TNBCs may be more active despite its low expression.

Mutations in SHP-2 affect phosphatase activity and are associated with diseases such as leukemia [18], Noonan syndrome, and LEOPARD syndrome [19]. Although two candidate sites were identified through CDS sequencing (Fig. S1C), validation demonstrated that they were not genuine mutations (Fig. 1G, S1D). Therefore, SHP-2 shows no significant variation or RNA editing across the cell lines.

Secondly, alternative splicing influences cancer development [20], but only one main band was detected (Fig. 1H). SHP-2 has an alternative splicing variant that is 12 bp longer than the canonical form, however, its expression was too low to quantify by RT-qPCR across several cell lines (data not shown). Additionally, no significant differences in cell migration or invasion were observed between the variants (Fig. S1E). Therefore, alternative splicing does not explain the expression discrepancy.

Post-translational modifications (PTMs) are crucial for protein function, with phosphorylation playing a key role in signal transduction [21]. Phosphorylation at tyrosine residues Y542 and Y580 of SHP-2 relieves its self-inhibitory conformation, thereby enhancing its phosphatase activity [22]. Interestingly, phosphorylation levels were higher in cell lines exhibiting low SHP-2 expression (Fig. 1I). Thus, increased phosphorylation may contribute to cell invasiveness and the observed

differences in SHP-2 expression.

To validate this, we measured SHP-2 phosphatase activity across several cell lines. Relative activity was significantly higher in low-expression lines (Fig. 1J). The correlation coefficients between relative phosphatase activity and total protein, as well as phosphorylation at Y542 and Y580, were -0.7, 0.6, and 0.6, respectively (Fig. 1K–1M). Phosphorylation at Y542 and Y580 showed a perfect correlation (r = 1.0; Fig. S1F). The phosphorylation levels in MDA-MB-468, HCC-1954, and BT-549 were notably higher (Fig. 1N), possibly due to positive feedback regulation.

ZEB1 Participates in the Positive Feedback Regulation of SHP-2 Y542 Phosphorylation

SHP-2 acts upstream, with EMT transcription factors serving as intermediates in cell migration and invasion. Using TCGA data accessed via GEPIA [23], we calculated Pearson correlation coefficients between them in cancers and normal tissues. The strong correlation between ZEBs and SHP-2 decreased from approximately 0.8 to 0.3 in breast cancer (Fig. 2A, 2B). ZEB1 was expressed at higher levels than ZEB2 (data not shown) and showed no significant splicing isoforms after long-term electrophoresis (Fig. 1I), therefore it was selected for further study. The correlation coefficients between ZEB1 and two phosphorylation sites were 0.58 and 0.81, respectively (Fig. 2C).

ZEB1 expression mirrored changes in SHP-2 during transient transfection (Fig. 2D, 2E). SHP-2's promotion of cell migration and invasion was dependent on ZEB1 (Fig. 2F). Stable *PTPN11* overexpression and knockdown cell lines were generated using lentiviral transduction. SHP-2 levels significantly increased only in MDA-MB-468 cells with overexpression, accompanied by increased ZEBs expression. However, ZEB expression varied following SHP-2 knockdown by shRNA (Fig. 2G), raising concerns about potential off-target effects. Two *PTPN11* knockout cell lines were generated using CRISPR/Cas9, as previously described [9]. Although slight compensation occurred in BT-549 PTPN11$^{-/-}$ cells (data not shown), SHP-2 levels were significantly decreased in both knockout lines. ZEB1 protein levels decreased in BT-549 PTPN11$^{-/-}$ but increased in T-47D PTPN11$^{-/-}$ cells (Fig. 2H, 2I), indicating that SHP-2 promotes ZEB1 expression in BT-549 but inhibits it in T-47D cells. Furthermore, ZEB1 overexpression and inhibition respectively increased and decreased phosphorylation at Y542 (Fig. 2J, 2K).

SHP-2 Initially Inhibits but Subsequently Increases ZEB1 Expression Through Multiple Pathways

SHP-2 increased ZEB1 expression by activating the PI3K/AKT and MEK/ERK pathways in PDGFRα-driven glioma cells during EMT and invasion [10]. It also enhanced SRC activation in endothelial cells [24], and SRC promoted YAP1 nuclear translocation and ZEB1 expression in squamous cell carcinomas [25]. Consistently, SHP-2 activated these pathways and elevated ZEB1 levels (Fig. 3A), which decreased when either pathway was inhibited by siRNAs or specific inhibitors (Fig. 3B, 3C). SHP-2 also significantly increased ZEB1 mRNA levels (Fig. 3D). Since ETS1, downstream of ERK [26, 27], and AP-1, downstream of AKT [28, 29], regulate ZEB1 transcription [30, 31]. ETS1, YAP1, and the AP-1 subunit JUN were further analyzed. All showed increased nuclear localization after SHP-2 overexpression (Fig. 3E). JASPAR [32] identified several potential binding sites, and ZEB1 promoter luciferase activity increased following transcription factor overexpression (Fig. S2A-S2C).

SHP-2 increases ZEB1 expression via the PI3K/AKT, MEK/ERK, and SRC/YAP1 pathways. Previous studies have reported that SHP-2 promotes SRC and AKT activation solely through its adaptor function, independent of its phosphatase activity [33, 34]. However, our results demonstrate that SHP-2's promotion of cell migration and invasion depends on both ZEB1 and its phosphatase

activity. Specifically, overexpression of the phosphatase-inactive mutant C459S failed to increase ZEB1 levels and inhibited all three pathways (Fig. 3F, S2D, S2E), indicating that ZEB1 expression and pathway activation require SHP-2 phosphatase activity. Additionally, inhibition of YAP1 and TAZ reduced ZEB1 expression despite SHP-2 overexpression (Fig. 3C). Since YAP1 and TAZ interact with SHP-2 to promote its nuclear localization [35], SHP-2 likely dephosphorylates nuclear substrates to enhance ZEB1 expression.

Parafibromin, encoded by *CDC73*, is a substrate of SHP-2 and cooperates with β-catenin in the nucleus to promote cancer development [36]. β-catenin levels increase via AKT-mediated inactivation of GSK-3β [37]. SHP-2 overexpression inactivated GSK-3β and elevated β-catenin levels (Fig. 3A), with a significant increase in nuclear β-catenin observed (Fig. 3E). Thus, parafibromin may regulate SHP-2-mediated ZEB1 expression. Overexpression of both wild-type (WT) and nuclear localization signal mutant parafibromin [38, 39] significantly decreased ZEB1 levles (Fig. 3G), while parafibromin inhibition also reduced ZEB1 expression (Fig. 3H) and suppressed ZEB1 despite SHP-2 overexpression (Fig. 3I). Parafibromin regulation by SHP-2 depends on the PI3K pathway (Fig. 3J). These findings indicate that parafibromin is essential for SHP-2 to increase ZEB1 in a specific form.

We examined the dynamic changes in downstream factors and phosphorylated parafibromin following SHP-2 overexpression. Phosphorylated parafibromin initially increased and then decreased, while ZEB1 showed the opposite pattern, decreasing early and subsequently increasing (Fig. 3K). This suggests that phosphorylated parafibromin inhibits ZEB1, whereas its dephosphorylated form promotes ZEB1 expression. Additionally, EMT-related genes displayed reversed expression patterns over time (Fig. 1F, S2F). Parafibromin also tended to degrade after dephosphorylation. Although Y290 was reported as SHP-2's primary target site [36], mutating this residue had no significant effect on ZEB1 levels (Fig. 3L). Purified SHP-2 was used to dephosphorylate parafibromin in vitro (Fig. S2G). Phos-tag SDS-PAGE revealed multiple bands, with the main band unaffected by SHP-2 dephosphorylation in both WT and Y290F mutants (Fig. 3M), indicating the presence of additional phosphorylation sites and that Y290 is not the primary SHP-2 target.

ZEB1 Enhances IL-6 mRNA Levels via Transcriptional and Post-transcriptional Regulation

Transcriptome sequencing identified 3,457 differentially expressed genes, including ZEB1, ZEB2, IL-6, and IL-8, which are highly expressed in BT-549 and MDA-MB-231 cells (Fig. 4A). Cytokine antibody array analysis showed IL-6 and IL-8 as the most abundantly and differentially secreted cytokines (Fig. 4B), with elevated levels observed across all TNBC samples (Fig. 4C, 4D, S3A, S3B). ZEB1 overexpression significantly increased IL-6 and IL-8 mRNA levels (Fig. 4E). Given that MCF-10A cells exhibit relatively high IL-8 expression but low Y542 phosphorylation, we mainly focused on IL-6. IL-6 stimulation also increased SHP-2 phosphorylation (Fig. 4F).

CUT&Tag sequencing revealed ZEB1 binding across the genome, with enrichment near the transcription start sites of genes primarily involved in cell movement (Fig. S3C, 3D). IL-6 and IL-8 were identified as direct ZEB1 targets (Fig. 4G). Luciferase activity significantly decreased when putative ZEB1 binding sites were deleted (Fig. 4H, S3E-3G), and ChIP-PCR confirmed significant binding near the E-box motif (Fig. 4I). Mutating two key sites further reduced luciferase activity (Fig. 4J, 4K), although the effect was milder in longer promoter sequences, possibly due to compensation by other transcription factors or atypical ZEB1 binding sites. EMSA showed no significant difference between wild-type and mutant probes, even with extensive base mutations

(Fig. S3I, S3J), suggesting that ZEB1 may bind stem-loop structures rather than E-box sequences. Indeed, mutations disrupting the stem-loop, as predicted by RNA-fold [40], reduced ZEB1's transcriptional activation, while restoring the stem-loop rescued this effect (Fig. 4L). These results indicate that ZEB1 enhances IL-6 transcription by binding to a stem-loop structure in the promoter.

IL-6 is an inflammatory and immune-related mRNA that is prone to degradation due to conserved cis-elements, such as stem-loop structures and AU-rich elements in its 3'UTR [41, 42]. We investigated whether ZEB1 stabilizes IL-6 mRNA post-transcriptionally. Indeed, ZEB1 overexpression increased the half-life IL-6 mRNA (Fig. 4M).

ZEB1 Activates the IL-6 Pathway, Primarily Enhancing SHP-2 Phosphorylation via Gp130

Several ZEB1 transcripts were detected in BT-549 cells (data not shown). We evaluated their ability to promote IL-6 transcription and secretion. The conventional splice variant, encoding 1,124 amino acids, was the most effective in increasing IL-6 mRNA levels (Fig. 5A); however, none of the variants enhanced IL-6 secretion (Fig. 5B). Further validation in BT-549 PTPN11$^{-/-}$ cells showed that a 40-fold reduction in IL-6 mRNA did not affect its secretion (Fig. 5C, 5D). Thus, ZEB1 increases IL-6 mRNA but not protein levels, suggesting a mechanism regulating IL-6 translation. Since the PI3K/mTOR pathway regulates translation, we tested related inhibitors. LY294002 decreased IL-6 and IL-8 translation, whereas rapamycin unexpectedly increased it (Fig. 5E, 5F). Therefore, IL-6 and IL-8 translation is PI3K-dependent but antagonistic to mTOR signaling.

SHP-2 phosphorylation increases with IL-6 stimulation and ZEB1 overexpression; however, IL-6 secretion is saturated due to translational regulation. Does ZEB1 truly regulate Y542 phosphorylation via the IL-6 pathway? CUT&Tag sequencing revealed ZEB1 enrichment at the promoter regions of gp130 (IL6ST) and IL6R (Fig. 5G). ZEB1 enhanced gp130 promoter activity but not that of IL6R (Fig. 5H, 5I), and increased gp130 mRNA and protein levels (Fig. 5J, 5K). Knockdown of gp130 reduced SHP-2 phosphorylation (Fig. 5L), and ZEB1 failed to promote SHP-2 phosphorylation when gp130 was inhibited (Fig. 5M). Thus, ZEB1 regulates IL-6 signaling primarily through gp130, not IL-6.

IL-6 signaling pathway is less active than the EGF signaling pathway due to limited receptor availability. IL6R is expressed at low levels in most cells, except in MDA-MB-231 cells (Fig. 1I), consistent with previous reports [43]. However, soluble IL6R (sIL6R) is present at concentrations of 30–70 ng/mL in human serum [44], and trans-activation may enhance pathway activation. Indeed, SHP-2 phosphorylation increased following the addition of sIL6R (Fig. 5N), and ZEB1 expression depended on both IL-6 and IL6R (Fig. 5O).

SHP-2 and JAK1 were previously considered separate downstream effectors of gp130 [45]. However, studies have shown that JAK1 and JAK2 can interact with and phosphorylate SHP-2 at residues Y304 and Y327 [46, 47]. To determine JAK1's role in SHP-2 activation, we found that JAK1 knockdown reduced ZEB1's ability to increase SHP-2 phosphorylation (Fig. 5P). Since STAT3 is another key factor in the IL-6 pathway and is reported to act downstream of SHP-2, we examined its involvement in ZEB1 regulation. Treatment with napabucasin significantly decreased ZEB1 expression (Fig. 5Q). Thus, we confirmed the existence of an IL-6/IL6R-gp130/JAK1/SHP-2/STAT3/ZEB1 regulatory loop in BT-549 cells.

SHP-2 Forms Homodimers through Intermolecular Disulfide and Secondary interactions

Phosphorylation at Y542 and Y580 positively correlates with SHP-2 phosphatase activity. Are these sites the direct determinants? We performed combined simulations of both sites (Fig. S4A). The SHP-2 Y542E and Y580E mutants exhibited higher phosphatase activity than other mutants.

Deletion of the C-terminal tail also increased SHP-2 activity compared to the wild type. Additionally, the SHP-2 FF mutant retained some phosphatase activity. Unexpectedly, the C459S mutant showed even higher activity than the SHP-2 FF mutant (Fig. 6A). What is the key determinant of phosphatase activity?

Chi Ben et al. demonstrated that both YAP1 and TAZ are required for SHP-2 nuclear localization, as both contain SHP-2 binding domains [35]. Thus, at least two SHP-2 molecules interact with them and enter the nucleus simultaneously. IL-6 downstream factors, such as STAT family members, function as transcriptional activators by forming dimers. To investigate SHP-2 dimerization, FLAG- and HA-tagged SHP-2 were co-expressed in *PTPN11* knockout cell lines, and both tags were detected by immunoprecipitation, albeit at low levels (Fig. 6B). SEC-MALS confirmed that SHP-2 predominantly exists as dimers, with a minor fraction as polymers (Fig. 6C). Disrupting SH2 domains and other sites affecting phosphatase activity altered SHP-2 conformation but did not prevent dimer formation (Fig. 6D, S4B). Diagonal electrophoresis under various denaturation conditions confirmed the presence of disulfide bonds in SHP-2 (Fig. 6E, S4C). Protein denaturation and non-reducing electrophoresis in multiple cell lines and purified protein further validated both intermolecular and intramolecular disulfide bonds (Fig. 6F, S4D), indicating that some SHP-2 dimers form via secondary interactions without intermolecular disulfides. SHP-2 contains ten cysteines distributed across its four domains. Fragment analysis showed all fragments could form intermolecular disulfide bonds independently (Fig. S4E, S4F). Mass spectrometry revealed at least 30 distinct disulfide bonds between cysteine residues (Fig. 6G, Supplementary Table3). Mutation of all cysteines abolished dimer formation in denaturing and non-reducing electrophoresis, confirming the role of intermolecular disulfides in dimerization (Fig. 6H). However, dimers persisted in native-PAGE after cysteine mutation, indicating that secondary interactions also contribute to dimerization (Fig. 6I).

C459, the enzyme center of SHP-2, forms disulfide bonds with C104, C174, C259, C333, C367, and C486. We tested whether oxidizing and reducing agents affect its enzymatic activity. Phosphatase activity decreased when the concentrations of redox reagent exceeded the buffering capacity, whereas reagents with low redox potential had no significant effect (Fig. 6J). These results indicated that SHP-2 phosphatase activity is directly regulated by disulfide bonds formation. Since disulfide bonds are regulated by protein disulfide isomerase (PDI) and mainly formed in the endoplasmic reticulum (ER), we performed mass spectrometry on SHP-2 immunoprecipitates. As expected, PDI family members and ER stress-related proteins were found to interact with SHP-2 (Fig. 6K), with P4HB interaction further validated (Fig. 6L). Additionally, SHP-2 was also detected in the ER fraction (Fig. 6M).

Phosphorylation of Y542 and Y580 Signals Degradation

Two phosphorylation site mimics were expressed at low levels in our experiments (Fig. 7A). A negative correlation between phosphorylation and total protein levels was observed in cell lines (Fig. 1I and 7B), suggesting that phosphorylation may promote protein degradation. Protein stability was measured in two cell lines following treatment with cycloheximide (CHX) and MG132; however, no significant differences were detected (Fig. 7C). We hypothesize that SHP-2 levels in BT-549 cells were too low, and phosphorylation levels in T-47D cells were too minimal to detect changes. Next, we overexpressed SHP-2 in BT-549 cells and assessed its stability. MG132 clearly stabilized SHP-2, and phosphorylation decreased as the protein degraded (Fig. 7D), indicating that SHP-2 tends to degrade after phosphorylation. Whether this degradation is ubiquitination-dependent

remains to be determined.

Y542 and Y580 are Phosphorylated by EPHA2 in BT-549 cells

The two phosphorylation sites are positively associated with phosphatase activity and degradation. EPHA2 has been reported to phosphorylate Y542 and Y580; however, its regulatory pathways and activation sites remain controversial [48-51]. EPHA2 is expressed in BT-549 cells but is barely detectable in T-47D cells (Fig. 8A, 8B), suggesting that it regulates phosphorylation in BT-549 but not in T-47D cells. Overexpression experiments confirmed that EPHA2 regulates SHP-2 phosphorylation in BT-549 cells (Fig. 8C). Since both sites are positively correlated and phosphorylated by EPHA2, we investigated their relationship. Overexpression of Y542 and Y580 mimic plasmids was performed in BT-549 and T-47D PTPN11$^{-/-}$ cells. To account for degradation trends, more stable mutants were used. Neither mutation affected phosphorylation of the other, indicating that their phosphorylation is independent and cell type-dependent (Fig. 8D).

To analyze EPHA2 activation, phosphorylation simulations of Y772 and S897 were conducted. Both sites increased SHP-2 phosphorylation. Y772 appeared to stabilize the protein indirectly, while S897 directly enhanced enzymatic activity (Fig. 8E). Phosphorylation of Y772 and S897 was mainly regulated by PI3K and ERK1/2, respectively, with PI3K also influencing S897 phosphorylation via the ERK1/2 pathway (Fig. 8F). Thus, EPHA2 phosphorylates SHP-2 following activation by S897 phosphorylation, a process reinforced by Y772 phosphorylation through both ERK1/2 and PI3K pathways.

Negative Coupled Pathways of SHP-2/ZEB1

A positive feedback loop between SHP-2 and ZEB1exists in certain cell lines, potentially leading to unchecked overactivation of downstream pathways that can damage cells. Therefore, coupled negative regulatory pathways are necessary to maintain cellular balance. SHP-2 levels were significantly lower at both the protein and mRNA levels in highly phosphorylated cell lines (Fig. 1C, 1D, 1I). While ZEB1 regulates SHP-2 protein degradation via phosphorylation, it is unclear whether it also affect SHP-2 mRNA. ZEB1 overexpression decreased SHP-2 mRNA levels (Fig. 9A), and ZEB1 was enriched at the SHP-2 promoter region (Fig. 9B). However, results showed that ZEB1 promoted SHP-2 transcription (Fig. 9C, 9D), suggesting that ZEB1 reduces SHP-2 mRNA through post-transcriptional regulation.

EPHA2 is identified as a potential ZEB1 target (Fig. 9B), with its mRNA levels decreasing following ZEB1 overexpression (Fig. 9E). Dual luciferase assays confirmed that ZEB1 inhibits EPHA2 transcription (Fig. 9F, 9G). At the protein level, EPHA2 phosphorylates and promotes SHP-2 degradation (Fig. 9H, 8C), while SHP-2 also facilitates EPHA2 degradation (Fig. 9I) via both proteasome-dependent and -independent pathways. SHP-2 dephosphorylates EPHA2 at tyrosine 772 (Y772), influencing its degradation (Fig. 9J), as well as at additional EPHA2 sites (Fig. 9K).

Time-Dependent Multilevel Regulation of SHP-2 Pathways

High IL-6 and IL-8 expression may induce phosphorylation at Y542 and Y580 in certain cells (Fig. 1I, 4C, S3A). However, HCC-1954 cells exhibit high SHP-2 phosphorylation despite low IL-6 levels, whereas MCF-10A cells show high IL-8 expression but low phosphorylation. What accounts for this discrepancy?

IL-6 and EGF synergistically promote cell migration [52]. EGF also activates PI3K and ERK1/2 via Gab1/SHP-2 recruitment [53], suggesting that SHP-2 phosphorylation is regulated by multiple pathways, including EGF. We assessed EGFR expression and phosphorylation across 10 cell lines. SHP-2 phosphorylation was generally higher in cell lines exhibiting elevated levels of IL-6, IL-8,

and phosphorylated EGFR (p-EGFR) (Fig. 1I). EGF stimulation increased SHP-2 phosphorylation (Fig. 10A). Furthermore, PDGFR-α and TGF-β also enhanced SHP-2 phosphorylation (Figs. 10B, 10C, S5A, S5B).

We then combined IL-6 and EGF stimulation. However, SHP-2 phosphorylation and downstream activation were lower than with single stimulation (Fig. 10D). This may be due to the MEK/ERK pathway being activated at different magnitudes and times [53, 54]. IL-6/SHP-2 activates MEK/ERK in two steps via GAB1 [55], suggesting time-dependent activation of SHP-2 and its downstream pathways. We examined related factors at multiple time points and found that IL-6 and EGF activate the pathway differently in both magnitude and timing. Combined stimulation enhanced the effect and shortened the activation time (Figs. 10E, 10F, S5C, S5D). Additionally, ZEB1 was initially inhibited and later increased by different stimulations (Figs. S5B, S5C).

Discussion

This study aims to elucidate the underlying mechanisms behind the discrepancies in SHP-2 activity and its role in regulating breast cancer cell migration and invasion. These discrepancies partly arise from the SHP-2/ZEB1 positive feedback loop and related inhibitory pathways. SHP-2 predominantly exists as homodimers. Finally, a multi-step, balanced model of SHP-2-mediated signaling pathways is proposed.

SHP-2/ZEB1 Positive Feedback Pathway

SHP-2 initially inhibits and later increases ZEB1 expression through the dynamic modulation of parafibromin. In the early stage, SHP-2-mediated activation of PI3K elevates parafibromin levels, which suppress ZEB1. Subsequently, SHP-2 dephosphorylates parafibromin, enabling its interaction with β-catenin to enhance ZEB1 expression. While both SHP-2 and PTK6 regulate downstream gene expression via parafibromin phosphorylation and dephosphorylation [56], our study shows that SHP-2 alone controls parafibromin's upregulation and dephosphorylation, highlighting its bidirectional regulatory role.

SHP-2 enhances ZEB1 transcription via multiple transcription factors acting on a promoter region within 4 kb, suggesting that this region functions as a super-enhancer. ETS1 was the most effective and is likely the primary regulator. A similar mechanism, in which a key transcription factor serves as the main regulator, has been observed and validated in hematopoiesis [57].

Akihiro Katsura et al. reported that ZEB1 promotes an inflammatory phenotype in breast cancer cells by increasing IL-6 and IL-8 production [58]. IL-6 enhances SHP-2 phosphorylation, facilitating breast cancer metastasis [59], while SHP-2 regulates IL-6 expression via NF-κB activation [60]. Our results show that ZEB1 elevates IL-6 and IL-8 mRNA levels through both transcriptional and post-transcriptional mechanisms. Several DNA-binding proteins [61], including the transcription factor CTCF [62], can also bind RNA, suggesting that ZEB1 may function as an RNA-binding protein. However, IL-6 and IL-8 translation is regulated by a PI3K-dependent but mTOR-competitive mechanism, rendering high mRNA levels redundant in some cancer cells. The key regulator linking SHP-2/ZEB1 and IL-6 is gp130, which is upregulated by ZEB1. Although traditionally considered weaker than the EGF pathway in cancer, the IL-6 pathway may become more active once bottlenecks are relieved. Additionally, the soluble IL-6 receptor (sIL6R) is widely present in vivo. IL-8 promotes glioma cell mesenchymal transition via NF-κB in an autocrine manner [63] and activates the PI3K/AKT, MEK/ERK, and JAK2/STAT3 pathways [64]. In our study, IL-8 is highly secreted and activates these pathways in some cells, but the key factor linking SHP-2/ZEB1 in this pathway remains to be identified.

SHP-2/ZEB1 pathway creates a sustained inflammatory microenvironment and may play a critical role in inflammation-related diseases. Karine Poussin et al. showed that the gp130/JAK1 pathway promotes the development of inflammatory hepatocellular adenoma (IHCA) [65]. High expression levels of ZEB1 and IL-6 characterize inflammatory breast cancer (IBC) [66]. This pathway may also influence chronic inflammatory diseases such as inflammatory bowel disease [67], asthma, inflammatory pulmonary disease, and systemic lupus erythematosus [68]. Additionally, cancers such as COAD, LUAD, LUSC, and STAD are likely regulated by this pathway, as indicated by significant changes in Pearson correlation coefficients between *PTPN11* and ZEBs in these cancers.

Coupled Negative Pathways Involving SHP-2 and ZEB1

Several negative regulatory pathways interact with the SHP-2/ZEB1 positive feedback loop. Continuous activation of SHP-2 reduces its protein levels due to degradation triggered by phosphorylation at tyrosine residues Y542 and Y580. Overexpression of ZEB1 also decreases SHP-2 mRNA levels. Additionally, ZEB1 suppresses EPHA2 by inhibiting its transcription, while SHP-2 promotes EPHA2 degradation through dephosphorylation at Y772. Finally, parafibromin, a key substrate of SHP-2, undergoes degradation following dephosphorylation.

Another issue concerns the expression of SHP-2 in MDA-MB-231 cells. Although its mRNA level is low, the protein level is higher than in most other cells. Given that IL-6, IL-8, and p-EGFR levels are relatively high, SHP-2 protein should be continuously activated and degraded to maintain low levels. However, the opposite occurs, suggesting that a mechanism in MDA-MB-231 cells that enhances translation efficiency to sustain elevated SHP-2 protein levels, potentially increasing the cells' invasive potential.

The network of positive and negative feedback pathways partially explains the discrepancies in SHP-2 expression. Further interconnected pathways need to be identified in future studies. Additionally, the cause of increased SHP-2 expression in other cell lines remains unclear.

Phosphorylation of SHP-2 at Y542 and Y580 is a Crucial Signaling Event

Phosphorylation of Y542 and Y580 activates SHP-2, but the primary site regulating its phosphatase activity remains controversial. Some studies identify pY542 as crucial [69], while others emphasize Y580 [70]. One study found that the cis-interaction between C-SH2 and pY542 mediates Y580 phosphorylation and downstream signaling in mouse embryonic fibroblasts, whereas the trans-interaction of N-SH2 regulates SHP-2 phosphatase activity [71].

Phosphorylation at the two sites occurs independently and correlates positively with phosphatase activity, though they are not direct determinants. SHP-2 phosphatase activity is directly regulated by disulfide bonds. Phosphorylation of Y542 and Y580 also correlates with SHP-2 degradation, suggesting these modifications influence its conformation and stability. In BT-549 cells, EPHA2 is the primary PTK responsible for Y542 and Y580 phosphorylation, while the PTKs involved in other cells, such as T-47D, remain unidentified.

Allostery in SHP-2 Homodimers Acts as a Functional Switch

SHP-2 can inhibit PI3K/AKT activation and suppress transcription factors such as AP-1, NFAT, and NF-κB when complexed with PD-1 [72, 73]. However, our study and others show that SHP-2 can also activate the PI3K/AKT and MEK/ERK pathways [10]. *PTPN11* knockout reduced ZEB1 expression in BT-549 cells but increased it in T-47D cells. SHP-2 overexpression initially inhibited, then increased ZEB1 in BT-549 cells. No mutations or significant splice variants were detected in 10 cell lines. Therefore, SHP-2 functions are context-dependent, suggesting that labeling *PTPN11*

strictly as an oncogene or tumor suppressor is inappropriate. SHP-2's role depends on its conformation.

Since its crystal structure was discovered in 1998 [6], SHP-2 was believed to adopt a self-inhibited conformation via interaction between its N-SH2 and PTP domains, remaining inactive at rest. Activation was thought to occur via intramolecular binding of phosphorylated Y542 and Y580 to N-SH2 and C-SH2, respectively [22], or through intermolecular interactions with SH2 domains of molecules like growth factor receptors (EGFR, PDGFR) or scaffolding adapters (IRS, GAB2, GRB2) [5]. Here, we show that SHP-2 forms homodimers stabilized by disulfide bonds and secondary interactions. The catalytic cysteine residue C459 forms disulfide bonds with several residues, and its activity is directly regulated by redox reactions. Since this cysteine is conserved in PTKs and PTPs, disulfide bond regulation offers a promising area for studying enzymatic activity.

Traditionally, SHP-2 was classified as either active or resting. However, we identified multiple active conformations, suggesting its diverse functions depend on these various states. SHP-2 likely shifts between transformations under different conditions, as maintaining a single conformation is energetically costly. This implies baseline activity across SHP-2 pathways and limits overall expression, explaining why only slight protein increases occur in high-expression stable cell lines. All conformations likely exist in different cells, so SHP-2's role in cancer cannot be judged solely by phosphatase activity. For example, T-47D cells show higher total SHP-2 phosphatase activity than BT-549 cells due to greater protein abundance despite lower relative activity. Conformational changes between dimers may be the primary regulatory mechanism, offering energy efficiency and adaptability, similar to STAT1 activation/inactivation [74]. Our study shows sustained SHP-2 activation triggers degradation to maintain balance, shifting cells to a new state distinct from the original, paralleling EMT and MET processes in cancer. These mechanisms contribute to cellular homeostasis in normal and malignant states. SHP-2's dual role in cancer depends on conformations composition rather than expression levels, partially explaining ZEBs disruption in SHP-2 knockdown and overexpression cell lines.

Disulfide bonds regulated by PDI partially control SHP-2 conformations. Several PDIs, along with ERO1L and P4HA1, interact with SHP-2, suggesting its role in redox signaling and ER stress regulation. Further research is needed to clarify SHP-2's role in these processes and its ER translocation—whether via a signal sequence or unconventional secretion. Another issue is SHP-2 dimer formation. We propose SHP-2 forms dimers in the ER immediately after translation, supported by limited tag detection in co-immunoprecipitation. Native gel electrophoresis and SEC-MALS detected no SHP-2 monomers. However, FRET analysis with different fluorescent tags failed to detect dimers [71], possibly due to the large distance between the protein's C-terminal tail and N-terminal region of the protein dimers.

Cell membrane receptors dimerize with homologous or heterologous partners during ligand-induced signal transmission, as seen with EGFR [75] and IL6R family members [45]. Dimerization also occurs in transcription factors like the STAT family [76] and AP1 complex [77]. Recently, proteins such as the p85 subunit of PI3K [78] and RAF family members [79] have been found to dimerize. Our study reveals that SHP-2 also forms dimers. The prevalence and significance of protein dimerization are likely underestimated and merit further investigation.

Multi-step Activation and Balanced Signal Transduction Hypothesis of SHP-2

Hannes Bongartz et al. demonstrated the time-dependent two-way activation of the IL-6-induced MAPK pathway by GAB1, with SHP-2 essential for the entire process [55]. Ralph Fritsch et

al. confirmed RAS-mediated activation of PI3Kα, PI3Kγ, and PI3Kδ, and RAC/CDC42-mediated activation of PI3Kβ [80]. SHP-2 also mediates signal transduction from multiple receptors [81]. Based on these studies and our data, we propose that SHP-2 regulates full activation of ERK1/2 and PI3K in a time-dependent manner. We hypothesize that SHP-2 is activated through multiple steps and plays a key role in balanced signal transduction by forming complexes with other factors and shuttling between various receptors or RTKs. The SHP-2 complex integrates multiple pathways, with downstream activation resulting from combined effects of multiple receptors.

The hypothesis is as follows (Fig. S6A-6D): stimulating factors like EGF, IL-6, IL-8, TGF, and PDGF synergistically alter the conformation and composition of the SHP-2 complex through recruitment and interaction. The SHP-2 complex then interacts with GRB2, activating PI3K and ERK1/2 via RAS. PI3K activation increases parafibromin, which inhibits ZEB1. Concurrently, PI3K phosphorylates phosphoinositol-4,5-bisphosphate (PIP2) to generate phosphoinositol-3,4,5-trisphosphate (PIP3) on the cell membrane. ERK phosphorylates GAB1 at S552, promoting its membrane localization through PH domain interaction with PIP3 [82], a process facilitated by SHP-2, which interacts with the p85 subunit of PI3K [83]. This explains why high EGF concentrations promote GAB1-SHP-2 membrane localization independent of the GAB1 PH domain [53], suggesting additional membrane localization signals ensure robust signal transduction. The SHP-2 complex, aided by GAB1, associates with focal adhesions (FAs) to activate SRC, FAK, and others. SHP-2 may activate SRC by dephosphorylating paxillin and dissociating Csk, a negative SRC regulator [84], or by regulating PAG/Cbp phosphorylation to limit Csk access to SFKs [85]. Subsequently, SRC and other regulators reactivate RAS and activate PI3Kβ via RAC, fully activating ERK1/2 and PI3K pathways [86, 87]. The SHP-2 complex then translocate to the nucleus along microtubules near focal adhesions [88], assisted by motor proteins like dynamin. In the nucleus, it dephosphorylates parafibromin, promoting ZEB1 transcription via ETS1, JUN, and YAP1/TAZ. At last, ZEB1 increases IL-6, IL-8, gp130, and inhibits EPHA2 transcription. Negative feedback pathways maintain cellular balance; for example, in BT-549 cells, EPHA2 activated by PI3K/AKT and MEK/ERK interacts with SHP-2 to phosphorylate SHP-2 at Y542 and Y580, promoting its degradation. SHP-2 also facilitates EPHA2 degradation via dephosphorylation. In contrast, in T-47D cells, SHP-2 is rapidly phosphorylated and dephosphorylated upon stimulation. The specific protein tyrosine kinases (PTKs) and phosphatases (PTPs) involved remain to be identified.

Related receptors or RTKs can inhibit downstream pathway activation by transmitting negative signals to the complex, regulating partial activation through combined effects. Early activation prepares for further activation, while synergistic effects accelerate and deepen downstream responses. Activation timing and intensity vary by cell types, with higher stimulator concentrations inducing faster, stronger responses if receptors are compatible. Murphy et al. identified c-Fos as a sensor for ERK1/2 signal duration, transcribed early in the process [54]. Synergistic neurite outgrowth induction by nerve growth factor or epidermal growth factor (EGF) and IL-6 in PC12 cells has been reported [89], and combined IL-6 and EGF treatment increased migration in T-47D breast cancer cells [52]. Protein abundance varies by cell type, affecting signal sensitivity. For example, platelet-derived growth factor (PDGF) induces sustained ERK1/2 activation in Swiss 3T3 fibroblasts, while EGF causes only transient phosphorylation [54]. Strong EGF stimulation recruits GAB1 to EGFR, whereas weak stimulation recruits GAB1 to PIP3 at the plasma membrane [53], correlating with full or transient ERK1/2 activation. High EGF concentrations prompt rapid initial activation, preparing for amplification without PI3K involvement, so PI3K inhibitors do not affect

ERK1/2 activation under these conditions [53]. However, in our study, PI3K inhibition significantly impacted ERK1/2 activation.

This study reveals only a fraction of the SHP-2 regulatory network. Signal transduction is a coordinated, unified process involving multiple pathways, with additional changes in other factors likely present. The conformational shifts in SHP-2 homodimers and the interplay of positive and negative pathways suggest multiple cellular equilibria, akin to the yin-yang concept in traditional Chinese medicine, which emphasizes the unity and exchange of opposites. The related mechanisms aim to maintain cellular balance and flexibility.

Conclusions

We identified an SHP-2/ZEB1-centered network contributing to the diverse expression of SHP-2 in breast cancer. We also found that SHP-2 primarily exists as dimers, with its structure and function regulated by disulfide bonds, secondary bonds, and other PTMs. These findings explain why *PTPN11* can act as either an oncogene or tumor suppressor depending on context. We propose that the SHP-2 complex mediates signal transduction via a multi-step, balanced mechanism.

Our detection of protein and mRNA changes was limited to one or a few time points, providing only a snapshot of their dynamic variations and failing to capture temporal changes across multiple pathways. More time points are needed to better understand the dynamic regulation of signal transduction. Additionally, due to differences in protein composition and abundance among cell types, specific checkpoints are necessary to clarify the interrelationships and dynamic changes of multiple pathways. However, we only used fixed time points between cell lines. Another limitation is the unclear relationship between JAK1/STAT3 and the other three pathways, which requires further investigation.

Further research is suggested to: (1) reveal structural and functional differences of SHP-2 dimers; (2) develop tools to visualize SHP-2 conformational changes; (3) determine how these conformations are regulated, especially by disulfide bonds and other different PTMs; (4) identify other components and their dynamic changes within the SHP-2 complex; (5) clarify whether gene function controversies in cancer are influenced by conformational differences; and (6) uncover additional integration complexes involved in signal transduction.

Acknowledgments The authors thank Professor Gao Xiaoqing for help in immunohistochemistry experiment. We are grateful to those companies for assisting and help, Yeasen Biotechnology in library construction, Beijing Novogene in transcriptome sequencing, Guangzhou Epibiotek in CUT&Tag sequencing, Beijing Biotech Pack Scientific in SEC-MALS, Shanghai Applied Protein Technology in mass spectrometry, Baizhen Biotechnologies in disulfide bond mass spectrometry analysis, Mabnus Biotech in protein purification, General Biol in sequence synthesis and Sanger sequencing, Cyagen Biosciences in construction of *PTPN11* knockout cell lines.

Authors' contributions BL and M. Yan designed the experiments, performed the experiments, analyzed the data, wrote and corrected the manuscript. All authors approved the final manuscript.

Funding This work was supported by the following funds: National Natural Science Foundation of China (82103064), Luzhou Science and Technology Program (2024JYJ067, 2018JYJ33), the Scientific Research Fund of Southwest Medical University (2024ZKY085).

Data availability All the data that support the findings are available from the corresponding author upon reasonable request.

Declarations

Ethics approval and consent to participate All experiments involving patient samples and related chips were approved by the Ethics Committee of Shanghai Outdo Biotech Company under project license number SHYJS-BC-2310001.

Consent for publication Not applicable.

Competing interests The authors declare no competing interests.

REFERENCES

1. Nolan E, Lindeman GJ, Visvader JE. Deciphering breast cancer: from biology to the clinic. **Cell 2023**, 186(8)**:** 1708-1728.
2. Hashim D, Boffetta P, La Vecchia C, Rota M, Bertuccio P, Malvezzi M*, et al.* The global decrease in cancer mortality: trends and disparities. **Ann Oncol 2016**, 27(5)**:** 926-933.
3. Entschladen F, Lindquist JA, Serfling E, Thiel G, Kieser A, Giehl K*, et al.* Signal transduction--receptors, mediators, and genes. **Sci Signal 2009**, 2(63).
4. Wang YT, Salter MW. Regulation of NMDA receptors by tyrosine kinases and phosphatases. **Nature 1994**, 369(6477)**:** 233-235.
5. Qu CK. The SHP-2 tyrosine phosphatase: signaling mechanisms and biological functions. **Cell Res 2000**, 10(4)**:** 279-288.
6. Hof P, Pluskey S, Dhe-Paganon S, Eck MJ, Shoelson SE. Crystal structure of the tyrosine phosphatase SHP-2. **Cell 1998**, 92(4)**:** 441-450.
7. Bard-Chapeau EA, Li S, Ding J, Zhang SS, Zhu HH, Princen F*, et al.* Ptpn11/Shp2 acts as a tumor suppressor in hepatocellular carcinogenesis. **Cancer Cell 2011**, 19(5)**:** 629-639.
8. Martin E, Agazie YM. SHP2 Potentiates the Oncogenic Activity of β-Catenin to Promote Triple-Negative Breast Cancer. **Mol Cancer Res 2021**, 19(11)**:** 1946-1956.
9. Yuan Y, Fan Y, Gao Z, Sun X, Zhang H, Wang Z*, et al.* SHP2 promotes proliferation of breast cancer cells through regulating Cyclin D1 stability via the PI3K/AKT/GSK3β signaling pathway. **Cancer Biol Med 2020**, 17(3)**:** 707-725.
10. Zhang L, Zhang W, Li Y, Alvarez A, Li Z, Wang Y*, et al.* SHP-2-upregulated ZEB1 is important for PDGFRα-driven glioma epithelial-mesenchymal transition and invasion in mice and humans. **Oncogene 2016**, 35(43)**:** 5641-5652.
11. Muenst S, Obermann EC, Gao F, Oertli D, Viehl CT, Weber WP*, et al.* Src homology phosphotyrosyl phosphatase-2 expression is an independent negative prognostic factor in human breast cancer. **Histopathology 2013**, 63(1)**:** 74-82.
12. Spandidos A, Wang X, Wang H, Seed B. PrimerBank: a resource of human and mouse PCR primer pairs for gene expression detection and quantification. **Nucleic Acids Res 2010**, 38(Database issue)**:** 11.
13. Sobotta MC, Liou W, Stöcker S, Talwar D, Oehler M, Ruppert T*, et al.* Peroxiredoxin-2 and STAT3 form a redox relay for H2O2 signaling. **Nat Chem Biol 2015**, 11(1)**:** 64-70.
14. Liu Y, Zuo Y, Li C, Fu P, He X, Wang Z*, et al.* Activation of an antifungal pathway in Yersinia pseudotuberculosis by chitin-receptor-mediated fungal recognition. **Curr Biol 2025**, 35(11)**:** 2672-2683.
15. Nelson JD, Denisenko O, Bomsztyk K. Protocol for the fast chromatin immunoprecipitation (ChIP) method. **Nat Protoc 2006**, 1(1)**:** 179-185.
16. Yue Q, Wang Z, Shen Y, Lan Y, Zhong X, Luo X*, et al.* Histone H3K9 Lactylation Confers Temozolomide Resistance in Glioblastoma via LUC7L2-Mediated MLH1 Intron Retention.

Adv Sci 2024, 11(19)**:** 13.

17. Kaya-Okur HS, Wu SJ, Codomo CA, Pledger ES, Bryson TD, Henikoff JG*, et al.* CUT&Tag for efficient epigenomic profiling of small samples and single cells. **Nat Commun 2019**, 10(1)**:** 019-09982.
18. Mohi MG, Williams IR, Dearolf CR, Chan G, Kutok JL, Cohen S*, et al.* Prognostic, therapeutic, and mechanistic implications of a mouse model of leukemia evoked by Shp2 (PTPN11) mutations. **Cancer Cell 2005**, 7(2)**:** 179-191.
19. Tartaglia M, Martinelli S, Stella L, Bocchinfuso G, Flex E, Cordeddu V*, et al.* Diversity and functional consequences of germline and somatic PTPN11 mutations in human disease. **Am J Hum Genet 2006**, 78(2)**:** 279-290.
20. Pradella D, Naro C, Sette C, Ghigna C. EMT and stemness: flexible processes tuned by alternative splicing in development and cancer progression. **Mol Cancer 2017**, 16(1)**:** 016-0579.
21. Olsen JV, Blagoev B, Gnad F, Macek B, Kumar C, Mortensen P*, et al.* Global, in vivo, and site-specific phosphorylation dynamics in signaling networks. **Cell 2006**, 127(3)**:** 635-648.
22. Lu W, Gong D, Bar-Sagi D, Cole PA. Site-specific incorporation of a phosphotyrosine mimetic reveals a role for tyrosine phosphorylation of SHP-2 in cell signaling. **Mol Cell 2001**, 8(4)**:** 759-769.
23. Tang Z, Li C, Kang B, Gao G, Li C, Zhang Z. GEPIA: a web server for cancer and normal gene expression profiling and interactive analyses. **Nucleic Acids Research 2017**, 45(W1)**:** W98-W102.
24. Yan M, Zhang X, Chen A, Gu W, Liu J, Ren X*, et al.* Endothelial cell SHP-2 negatively regulates neutrophil adhesion and promotes transmigration by enhancing ICAM-1-VE-cadherin interaction. **Faseb J 2017**, 31(11)**:** 4759-4769.
25. Pastushenko I, Mauri F, Song Y, de Cock F, Meeusen B, Swedlund B*, et al.* Fat1 deletion promotes hybrid EMT state, tumour stemness and metastasis. **Nature 2021**, 589(7842)**:** 448-455.
26. Yang L, Zheng L, Chng WJ, Ding JL. Comprehensive Analysis of ERK1/2 Substrates for Potential Combination Immunotherapies. **Trends Pharmacol Sci 2019**, 40(11)**:** 897-910.
27. Plotnik JP, Budka JA, Ferris MW, Hollenhorst PC. ETS1 is a genome-wide effector of RAS/ERK signaling in epithelial cells. **Nucleic Acids Res 2014**, 42(19)**:** 11928-11940.
28. Pan CH, Chen SY, Wang JY, Tsao SP, Huang HY, Wei-Chen Chiu P*, et al.* Sclareol ameliorated ERCC1-mediated cisplatin resistance in A549 human lung adenocarcinoma cells and a murine xenograft tumor model by suppressing AKT-GSK3β-AP1/Snail and JNK-AP1 pathways. **Chem Biol Interact 2020**, 332(109304)**:** 24.
29. Song Y, Zhao M, Zhang H, Yu B. Double-edged roles of protein tyrosine phosphatase SHP2 in cancer and its inhibitors in clinical trials. **Pharmacol Ther 2022**, 230(107966)**:** 14.
30. Sinh ND, Endo K, Miyazawa K, Saitoh M. Ets1 and ESE1 reciprocally regulate expression of ZEB1/ZEB2, dependent on ERK1/2 activity, in breast cancer cells. **Cancer Sci 2017**, 108(5)**:** 952-960.
31. Bakiri L, Macho-Maschler S, Custic I, Niemiec J, Guío-Carrión A, Hasenfuss SC*, et al.* Fra-1/AP-1 induces EMT in mammary epithelial cells by modulating Zeb1/2 and TGFβ expression. **Cell Death Differ 2015**, 22(2)**:** 336-350.
32. Rauluseviciute I, Riudavets-Puig R, Blanc-Mathieu R, Castro-Mondragon JA, Ferenc K, Kumar V*, et al.* JASPAR 2024: 20th anniversary of the open-access database of transcription factor

binding profiles. **Nucleic Acids Res 2024**, 52(D1)**:** D174-D182.

33. Walter AO, Peng ZY, Cartwright CA. The Shp-2 tyrosine phosphatase activates the Src tyrosine kinase by a non-enzymatic mechanism. **Oncogene 1999**, 18(11)**:** 1911-1920.
34. Wu CJ, O'Rourke DM, Feng GS, Johnson GR, Wang Q, Greene MI. The tyrosine phosphatase SHP-2 is required for mediating phosphatidylinositol 3-kinase/Akt activation by growth factors. **Oncogene 2001**, 20(42)**:** 6018-6025.
35. Ben C, Wu X, Takahashi-Kanemitsu A, Knight CT, Hayashi T, Hatakeyama M. Alternative splicing reverses the cell-intrinsic and cell-extrinsic pro-oncogenic potentials of YAP1. **J Biol Chem 2020**, 295(41)**:** 13965-13980.
36. Takahashi A, Tsutsumi R, Kikuchi I, Obuse C, Saito Y, Seidi A*, et al.* SHP2 tyrosine phosphatase converts parafibromin/Cdc73 from a tumor suppressor to an oncogenic driver. **Mol Cell 2011**, 43(1)**:** 45-56.
37. Marineau A, Khan KA, Servant MJ. Roles of GSK-3 and β-Catenin in Antiviral Innate Immune Sensing of Nucleic Acids. **Cells 2020**, 9(4).
38. Hahn MA, Marsh DJ. Identification of a functional bipartite nuclear localization signal in the tumor suppressor parafibromin. **Oncogene 2005**, 24(41)**:** 6241-6248.
39. Wei J, Lian H, Zhong B, Shu HB. Parafibromin Is a Component of IFN-γ-Triggered Signaling Pathways That Facilitates JAK1/2-Mediated Tyrosine Phosphorylation of STAT1. **J Immunol 2015**, 195(6)**:** 2870-2878.
40. Lorenz R, Bernhart SH, Höner Zu Siederdissen C, Tafer H, Flamm C, Stadler PF*, et al.* ViennaRNA Package 2.0. **Algorithms Mol Biol 2011**, 6(26)**:** 1748-7188.
41. Kafasla P, Skliris A, Kontoyiannis DL. Post-transcriptional coordination of immunological responses by RNA-binding proteins. **Nat Immunol 2014**, 15(6)**:** 492-502.
42. Mino T, Murakawa Y, Fukao A, Vandenbon A, Wessels HH, Ori D*, et al.* Regnase-1 and Roquin Regulate a Common Element in Inflammatory mRNAs by Spatiotemporally Distinct Mechanisms. **Cell 2015**, 161(5)**:** 1058-1073.
43. Kang S, Narazaki M, Metwally H, Kishimoto T. Historical overview of the interleukin-6 family cytokine. **J Exp Med 2020**, 217(5)**:** 20190347.
44. Riethmueller S, Somasundaram P, Ehlers JC, Hung CW, Flynn CM, Lokau J*, et al.* Proteolytic Origin of the Soluble Human IL-6R In Vivo and a Decisive Role of N-Glycosylation. **PLoS Biol 2017**, 15(1).
45. Jones SA, Jenkins BJ. Recent insights into targeting the IL-6 cytokine family in inflammatory diseases and cancer. **Nat Rev Immunol 2018**, 18(12)**:** 773-789.
46. Yin T, Shen R, Feng GS, Yang YC. Molecular characterization of specific interactions between SHP-2 phosphatase and JAK tyrosine kinases. **J Biol Chem 1997**, 272(2)**:** 1032-1037.
47. Schaper F, Gendo C, Eck M, Schmitz J, Grimm C, Anhuf D*, et al.* Activation of the protein tyrosine phosphatase SHP2 via the interleukin-6 signal transducing receptor protein gp130 requires tyrosine kinase Jak1 and limits acute-phase protein expression. **Biochem J 1998**, 335(Pt 3)**:** 557-565.
48. Miura K, Wakayama Y, Tanino M, Orba Y, Sawa H, Hatakeyama M*, et al.* Involvement of EphA2-mediated tyrosine phosphorylation of Shp2 in Shp2-regulated activation of extracellular signal-regulated kinase. **Oncogene 2013**, 32(45)**:** 5292-5301.
49. Miao H, Li DQ, Mukherjee A, Guo H, Petty A, Cutter J*, et al.* EphA2 mediates ligand-dependent inhibition and ligand-independent promotion of cell migration and invasion via a reciprocal

regulatory loop with Akt. **Cancer Cell 2009**, 16(1)**:** 9-20.

50. Zhou Y, Yamada N, Tanaka T, Hori T, Yokoyama S, Hayakawa Y*, et al.* Crucial roles of RSK in cell motility by catalysing serine phosphorylation of EphA2. **Nat Commun 2015**, 6(7679).
51. Xiang YP, Xiao T, Li QG, Lu SS, Zhu W, Liu YY*, et al.* Y772 phosphorylation of EphA2 is responsible for EphA2-dependent NPC nasopharyngeal carcinoma growth by Shp2/Erk-1/2 signaling pathway. **Cell Death Dis 2020**, 11(8)**:** 020-02831.
52. Badache A, Hynes NE. Interleukin 6 inhibits proliferation and, in cooperation with an epidermal growth factor receptor autocrine loop, increases migration of T47D breast cancer cells. **Cancer Res 2001**, 61(1)**:** 383-391.
53. Sampaio C, Dance M, Montagner A, Edouard T, Malet N, Perret B*, et al.* Signal strength dictates phosphoinositide 3-kinase contribution to Ras/extracellular signal-regulated kinase 1 and 2 activation via differential Gab1/Shp2 recruitment: consequences for resistance to epidermal growth factor receptor inhibition. **Mol Cell Biol 2008**, 28(2)**:** 587-600.
54. Murphy LO, Smith S, Chen RH, Fingar DC, Blenis J. Molecular interpretation of ERK signal duration by immediate early gene products. **Nat Cell Biol 2002**, 4(8)**:** 556-564.
55. Bongartz H, Gille K, Hessenkemper W, Mandel K, Lewitzky M, Feller SM*, et al.* The multi-site docking protein Grb2-associated binder 1 (Gab1) enhances interleukin-6-induced MAPK-pathway activation in an SHP2-, Grb2-, and time-dependent manner. **Cell Commun Signal 2019**, 17(1)**:** 019-0451.
56. Tang C, Takahashi-Kanemitsu A, Kikuchi I, Ben C, Hatakeyama M. Transcriptional Co-activator Functions of YAP and TAZ Are Inversely Regulated by Tyrosine Phosphorylation Status of Parafibromin. **iScience 2018**, 2(103)**:** 12.
57. Huang J, Liu X, Li D, Shao Z, Cao H, Zhang Y*, et al.* Dynamic Control of Enhancer Repertoires Drives Lineage and Stage-Specific Transcription during Hematopoiesis. **Dev Cell 2016**, 36(1)**:** 9-23.
58. Katsura A, Tamura Y, Hokari S, Harada M, Morikawa M, Sakurai T*, et al.* ZEB1-regulated inflammatory phenotype in breast cancer cells. **Mol Oncol 2017**, 11(9)**:** 1241-1262.
59. Sun X, Zhang J, Wang Z, Ji W, Tian R, Zhang F*, et al.* Shp2 Plays a Critical Role in IL-6-Induced EMT in Breast Cancer Cells. **Int J Mol Sci 2017**, 18(2).
60. You M, Flick LM, Yu D, Feng GS. Modulation of the nuclear factor kappa B pathway by Shp-2 tyrosine phosphatase in mediating the induction of interleukin (IL)-6 by IL-1 or tumor necrosis factor. **J Exp Med 2001**, 193(1)**:** 101-110.
61. Cassiday LA, Maher LJ, 3rd. Having it both ways: transcription factors that bind DNA and RNA. **Nucleic Acids Res 2002**, 30(19)**:** 4118-4126.
62. Kung JT, Kesner B, An JY, Ahn JY, Cifuentes-Rojas C, Colognori D*, et al.* Locus-specific targeting to the X chromosome revealed by the RNA interactome of CTCF. **Mol Cell 2015**, 57(2)**:** 361-375.
63. Zhang B, Shi L, Lu S, Sun X, Liu Y, Li H*, et al.* Autocrine IL-8 promotes F-actin polymerization and mediate mesenchymal transition via ELMO1-NF-κB-Snail signaling in glioma. **Cancer Biol Ther 2015**, 16(6)**:** 898-911.
64. Waugh DJ, Wilson C. The interleukin-8 pathway in cancer. **Clin Cancer Res 2008**, 14(21)**:** 6735-6741.
65. Poussin K, Pilati C, Couchy G, Calderaro J, Bioulac-Sage P, Bacq Y*, et al.* Biochemical and functional analyses of gp130 mutants unveil JAK1 as a novel therapeutic target in human

inflammatory hepatocellular adenoma. **Oncoimmunology 2013**, 2(12)**:** 3.

66. Lim B, Woodward WA, Wang X, Reuben JM, Ueno NT. Inflammatory breast cancer biology: the tumour microenvironment is key. **Nat Rev Cancer 2018**, 18(8)**:** 485-499.
67. Rosen MJ, Dhawan A, Saeed SA. Inflammatory Bowel Disease in Children and Adolescents. **JAMA Pediatr 2015**, 169(11)**:** 1053-1060.
68. Yao X, Huang J, Zhong H, Shen N, Faggioni R, Fung M*, et al.* Targeting interleukin-6 in inflammatory autoimmune diseases and cancers. **Pharmacol Ther 2014**, 141(2)**:** 125-139.
69. Bennett AM, Tang TL, Sugimoto S, Walsh CT, Neel BG. Protein-tyrosine-phosphatase SHPTP2 couples platelet-derived growth factor receptor beta to Ras. **Proc Natl Acad Sci U S A 1994**, 91(15)**:** 7335-7339.
70. Keegan K, Cooper JA. Use of the two hybrid system to detect the association of the protein-tyrosine-phosphatase, SHPTP2, with another SH2-containing protein, Grb7. **Oncogene 1996**, 12(7)**:** 1537-1544.
71. Sun J, Lu S, Ouyang M, Lin LJ, Zhuo Y, Liu B*, et al.* Antagonism between binding site affinity and conformational dynamics tunes alternative cis-interactions within Shp2. **Nat Commun 2013**, 4(2037).
72. Hui E, Cheung J, Zhu J, Su X, Taylor MJ, Wallweber HA*, et al.* T cell costimulatory receptor CD28 is a primary target for PD-1-mediated inhibition. **Science 2017**, 355(6332)**:** 1428-1433.
73. Liu Q, Qu J, Zhao M, Xu Q, Sun Y. Targeting SHP2 as a promising strategy for cancer immunotherapy. **Pharmacol Res 2020**, 152(104595)**:** 12.
74. Haspel RL, Salditt-Georgieff M, Darnell JE, Jr. The rapid inactivation of nuclear tyrosine phosphorylated Stat1 depends upon a protein tyrosine phosphatase. **Embo J 1996**, 15(22)**:** 6262-6268.
75. Yarden Y, Sliwkowski MX. Untangling the ErbB signalling network. **Nat Rev Mol Cell Biol 2001**, 2(2)**:** 127-137.
76. Li YJ, Zhang C, Martincuks A, Herrmann A, Yu H. STAT proteins in cancer: orchestration of metabolism. **Nat Rev Cancer 2023**, 23(3)**:** 115-134.
77. Lopez-Bergami P, Lau E, Ronai Z. *Emerging roles of ATF2 and the dynamic AP1 network in cancer*. Nat Rev Cancer. 2010 Jan;10(1):65-76. doi: 10.1038/nrc2681.
78. Fox M, Mott HR, Owen D. Class IA PI3K regulatory subunits: p110-independent roles and structures. **Biochem Soc Trans 2020**, 48(4)**:** 1397-1417.
79. Lavoie H, Li JJ, Thevakumaran N, Therrien M, Sicheri F. Dimerization-induced allostery in protein kinase regulation. **Trends Biochem Sci 2014**, 39(10)**:** 475-486.
80. Fritsch R, de Krijger I, Fritsch K, George R, Reason B, Kumar MS*, et al.* RAS and RHO families of GTPases directly regulate distinct phosphoinositide 3-kinase isoforms. **Cell 2013**, 153(5)**:** 1050-1063.
81. Heinrich PC, Behrmann I, Müller-Newen G, Schaper F, Graeve L. Interleukin-6-type cytokine signalling through the gp130/Jak/STAT pathway. **Biochem J 1998**, 334(Pt 2)**:** 297-314.
82. Eulenfeld R, Schaper F. A new mechanism for the regulation of Gab1 recruitment to the plasma membrane. **J Cell Sci 2009**, 122(Pt 1)**:** 55-64.
83. Breitkopf SB, Yang X, Begley MJ, Kulkarni M, Chiu YH, Turke AB*, et al.* A Cross-Species Study of PI3K Protein-Protein Interactions Reveals the Direct Interaction of P85 and SHP2. **Sci Rep 2016**, 6(20471).
84. Ren Y, Meng S, Mei L, Zhao ZJ, Jove R, Wu J. Roles of Gab1 and SHP2 in paxillin tyrosine

dephosphorylation and Src activation in response to epidermal growth factor. **J Biol Chem 2004**, 279(9)**:** 8497-8505.

85. Zhang SQ, Yang W, Kontaridis MI, Bivona TG, Wen G, Araki T*, et al.* Shp2 regulates SRC family kinase activity and Ras/Erk activation by controlling Csk recruitment. **Mol Cell 2004**, 13(3)**:** 341-355.
86. Martin GS. The hunting of the Src. **Nat Rev Mol Cell Biol 2001**, 2(6)**:** 467-475.
87. Berton G, Mócsai A, Lowell CA. Src and Syk kinases: key regulators of phagocytic cell activation. **Trends Immunol 2005**, 26(4)**:** 208-214.
88. Fang X, Svitkina TM. Adenomatous Polyposis Coli (APC) in cell migration. **Eur J Cell Biol 2022**, 101(3)**:** 22.
89. Wu YY, Bradshaw RA. Synergistic induction of neurite outgrowth by nerve growth factor or epidermal growth factor and interleukin-6 in PC12 cells. **J Biol Chem 1996**, 271(22)**:** 13033-13039.

Figure 1. SHP-2 is expressed at low levels but undergoes highly tyrosine phosphorylation in certain cell lines. (A) Immunoblotting of SHP-2 in normal (N) and breast cancer tumor (T) tissues; GAPDH as loading control. (B) Representative images of SHP-2 immunohistochemical staining in breast cancer tissue microarrays (HBreD090CS01, BreD060CS05, OUTDO, Shanghai, China). (C) Immunoblotting of SHP-2 in a normal breast epithelial cell line and nine breast cancer cell lines. (D) Real-time PCR of SHP-2 mRNA in indicated cell lines. (E) BT-549 cell migration and Matrigel invasion assays after transfection with pcDNA 3.1 (Vector), SHP-2 WT, or SHP-2 C459S. (F) Immunoblotting of indicated proteins after FLAG-SHP-2 overexpression for 60 hours in BT-549 cells. (G) DNA Sanger sequencing of c.A106 and c.A1035 in indicated cell lines. (H) Immunoblotting of SHP-2 in BT-549 and T-47D cells. (I) Immunoblotting of indicated proteins in specified cell lines. (J) Relative SHP-2 activity in indicated cell lines. (K–M) Spearman correlations between SHP-2 activity and SHP-2 (K), p-SHP-2 (Y542) (L), or p-SHP-2 (Y580) (M) protein levels. (N) Relative p-SHP-2 (Y542) protein level normalized to SHP-2 in indicated cell lines.

Figure 2. ZEB1 participates in the positive feedback regulation of SHP-2 Y542 phosphorylation. (A) Pearson correlation between PTPN11 and EMT transcription factors in breast cancer from GEPIA. (B) Pearson correlation between PTPN11 and ZEBs across multiple cancers from GEPIA, (BRCA, breast invasive carcinoma, COAD, colon adenocarcinoma, HNSC, head and neck squamous cell carcinoma, KIRC, kidney renal clear cell carcinoma, KIRP, kidney renal papillary cell carcinoma, LIHC, liver hepatocellular carcinoma, LUAD, lung adenocarcinoma, LUSC, lung squamous cell carcinoma, PRAD, prostate adenocarcinoma, STAD, stomach adenocarcinoma, THCA, thyroid carcinoma). (C) Spearman correlation between ZEB1 and p-SHP-2 (Y542 or Y580) protein levels. (D, E) Immunoblotting of SHP-2 and ZEB1 after SHP-2 overexpression (D) or knockdown (E) for 60 h in BT-549 cells. (F) Representative images of BT-549 cell migration and Matrigel invasion assays after transient transfection with Vector (pcDNA 3.1 and NC), SHP-2 (SHP-2 and NC), or SHP-2 plus siZEB1#3. (G) Immunoblotting of SHP-2, ZEB1, and ZEB2 after SHP-2 overexpression or knockdown virus infected MDA-MB-468, MDA-MB-231, MDA-MB-361, or T-47D cells, with quantification (bottom). (H) Immunoblotting of ZEB1 and ZEB2 in WT and PTPN11$^{-/-}$ BT-549 or T-47D cells. (I) Real-time PCR analysis of SHP-2, ZEB1, and ZEB2 expression in WT and PTPN11$^{-/-}$ BT-549 or T-47D cells. (J, K) Immunoblotting of ZEB1, p-Y542 SHP-2, and SHP-2 after ZEB1 overexpression (J) or knockdown (K) for 54 h in BT-549 cells.

Figure 3. SHP-2 initially inhibits but subsequently increases ZEB1 expression through multiple pathways. (A) Immunoblotting of indicated proteins after 60 h SHP-2 overexpression in BT-549 cells. (B) Immunoblotting of indicated proteins after 4.5 h treatment with DMSO, PD98059 (MEK inhibitor, MCE), or LY294002 (PI3K inhibitor, MCE) after serum starvation overnight. (C) Immunoblotting after 56 h SHP-2 overexpression or co-transfection with SHP-2 and YAP1/TAZ siRNA. (D) Real-time PCR of ZEB1 after 32 h SHP-2 overexpression. (E) Immunoblotting of cytoplasmic and nuclear fractions after 68 h SHP-2 overexpression; GAPDH and Histone H3 as markers. (F) Quantification of ZEB1 and p-Src in cells transfected with FLAG-SHP-2 C459S (see S3D). (G, H) Immunoblotting of ZEB1 and CDC73 after 52 h transfection with HA-CDC73, HA-CDC73 NLS mutant, or CDC73 siRNA. (I) Immunoblotting of indicated proteins after SHP-2 overexpression, or SHP-2 and CDC73 siRNA co-transfection for 52 h. (J) Immunoblotting of indicated proteins in BT-549 cells treated with DMSO, PD98059, or LY294002 for 4.5 h after serum starvation overnight. (K) Immunoblotting of the indicated protein levels and CDC73

phosphorylation detected by Phos-tag SDS-PAGE at various times post SHP-2 overexpression. (L) Immunoblotting of ZEB1 after 52 h transfection with HA-CDC73-290E or HA-CDC73-290F in BT-549 cells. (M) Whole-cell lysates from BT-549 cells transfected with HA-CDC73-WT (left) or HA-CDC73-290F (right) for 52 h incubated with purified SHP-2 at varying concentrations for 30 min at 37°C; phosphorylated CDC73 or CDC73-290F analyzed by Phos-tag SDS-PAGE.

Figure 4. ZEB1 enhances IL-6 mRNA via transcriptional and post-transcriptional regulation. (A) Number of differentially expressed genes in the transcriptomes of various cell lines. (B) Cytokine expression in conditioned media from breast cancer cell lines detected by Human Cytokine Array V; red boxes highlight IL-6 (left) and IL-8 (right). (C, D) ELISA for IL-6 concentration (C) and real-time PCR for IL-6 mRNA (D) in indicated cell lines. (E) Real-time PCR of IL-6, IL-8, and ZEB1 in BT-549 cells transfected with ZEB1 for 24 h (left) or 36 h (right). (F) Immunoblotting analysis of p-SHP-2 (Y542) and SHP-2 in BT-549 (left) and T-47D (right) cells after overnight serum starvation and 6 h IL-6 treatment. (G) Genomic tracks comparing ZEB1 and control at IL-6 and IL-8 promoter regions. (H) Luciferase assays in BT-549 cells transfected with IL-6-Luc promoter, pRL-TK (*Renilla* luciferase reporter), and FLAG-ZEB1 or empty vector for 52 h. (I) ChIP analysis of ZEB1 binding to IL-6 promoter in vivo; rabbit IgG and Histone H3 served as negative and positive controls. (J) Schematic diagram of wild-type and mutant IL-6 Pro-2 and Pro-5 promoter fragments. (K) Luciferase assays of BT-549 cells transfected with indicated IL-6-Luc promoter plasmids and pRL-TK for 52 h. (L) Fragment sequences, secondary structure analysis of IL-6-Pro5 wild-type and mutant, and luciferase assays in BT-549 cells transfected with promoter plasmids, pRL-TK, and FLAG-ZEB1 or FLAG-ZEB2 for 52 h. (M) Real-time PCR of IL-6 in BT-549 cells transfected with ZEB1 for 48 h, then treated with ActD (5 μg/mL) for indicated times.

Figure 5. ZEB1 activates the IL-6 pathway, primarily enhancing SHP-2 phosphorylation via gp130. (A) Luciferase reporter assays were performed on BT-549 cells transfected with IL-6-Pro-2 plasmid, pRL-TK, and FLAG-ZEB1 or empty vector for 52 h. (B) ELISA measured IL-6 levels in BT-549 cells after ZEB1 transfection for 52 h. (C, D) Real-time PCR and ELISA assessed IL-6 mRNA (C) and protein (D) in specified cells. (E, F) ELISA and immunoblotting evaluated IL-6, IL-8, and protein levels in BT-549 WT and PTPN11$^{-/-}$ cells after overnight serum starvation and 6 h treatment with DMSO, LY294002 (E), or Rapamycin (F). (G) Genomic tracks compared ZEB1 and control at IL6ST and IL6R promoters. (H, I) Luciferase assays of BT-549 cells transfected with gp130-Luc (H) or IL-6R-Luc (I), pRL-TK, and FLAG-ZEB1 or empty vector for 52 h; transcription start sites ENST00000381298.7 and ENST00000368485.8 marked +1. (J) Immunoblotting of ZEB1 and gp130 in BT-549 cells transfected with ZEB1 plasmid at indicated times. (K) Real-time PCR measured ZEB1 and gp130 expression after 48 h ZEB1 overexpression and 12 h medium replacement before RNA extraction. (L, M) Immunoblotting of indicated proteins in BT-549 cells transfected with sigp130 or siNC (L), or ZEB1 plasmid with sigp130 or siNC for 54 h (M). (N) Immunoblotting of p-SHP-2 (Y542), SHP2, and ZEB1 in BT-549 cells after overnight serum starvation followed by 12 h sIL-6R stimulation. (O) Immunoblotting of indicated proteins in BT-549 cells transfected with siIL-6R or siNC for 48 h, then treated with medium or IL-6 for 6 h. (P) Immunoblotting of indicated proteins in BT-549 cells transfected with ZEB1 plasmid, empty vector, siJAK1, or siNC for 52 h. (Q) Immunoblotting of indicated proteins after BT-549 cells underwent overnight serum starvation, followed by 6 h treatment with DMSO or Napabucasin (3.33 μM, STAT3 inhibitor, Target Mol).

Figure 6. SHP-2 phosphatase activity is directly regulated by disulfide bonds, and SHP-2 forms homodimers through intermolecular disulfide and secondary interactions. (A) SHP-2 phosphatase activity in BT-549 cells transfected with indicated plasmids for 52 h post-IP. (B) IP and Western blot of proteins in BT-549 and T-47D PTPN11$^{-/-}$ cells transfected with HA-SHP-2 and FLAG-SHP-2 plasmids. (C) SEC-MALS molecular weight and characterization of purified SHP-2. (D) Western blot (Native-PAGE) of FLAG-SHP-2 variants in BT-549 cells transfected with FLAG-SHP-2-62E, -62F, -73A, -73D, -R32E, -R138E, and -R32ER138E plasmids. (E) Whole-cell lysates from BT-549 and T-47D cells analyzed by diagonal gel electrophoresis, blotted and probed with anti-SHP-2; denatured at 100°C for 10 min. (F) Denaturing non-reducing electrophoresis of SHP-2 in BT-549 and T-47D cells (left: no DTT; right: with DTT; D, dimer; P, polymer; M, monomer). (G) Secondary mass spectrum of disulfide-bonded peptide segments from purified SHP-2. (H) Denaturing non-reducing electrophoresis of SHP-2 from BT-549 cells transfected with FLAG-SHP-2 WT (top) or FLAG-SHP-2 CS all (bottom) (left: no DTT; right: with DTT). (I) Native-PAGE of SHP-2 from BT-549 cells transfected with FLAG-SHP-2 WT or FLAG-SHP-2 CS all. (J) Phosphatase activity of purified SHP-2 treated with GSH, DTT, $K_2Cr_2O_7$, or H_2O_2 at indicated concentrations for 30 min at 37°C. (K) List of SHP-2-interacting proteins in BT-549 cells identified by mass spectrometry. (L) IP and Western blot of P4HB and SHP-2 in BT-549 and T-47D cells. (M) Immunoblot of P4HB and SHP-2 in endoplasmic reticulum fractions from BT-549 and T-47D cells; Calreticulin as loading control.

Figure 7. Phosphorylation of Y542 and Y580 signals degradation. (A) Immunoblotting of FLAG-SHP-2 in BT-549 cells transfected with wild-type (WT) or mutant SHP-2 plasmids. (B) Spearman correlation between SHP-2 protein levels and p-SHP-2 (Y542). (C, D) Immunoblotting of indicated proteins in BT-549 and T-47D cells (C), or BT-549 cells transfected with SHP-2 (D), treated with MG132 or CHX plus MG132 at specified time points.

Figure 8. Y542 and Y580 are phosphorylated by EPHA2 in BT-549 cells. (A, B) Real-time PCR analysis of EPHA2 levels (A) and immunoblotting of EPHA2 (B) in BT-549 and T-47D cells. (C) Immunoblotting of indicated proteins in BT-549 cells transfected with EPHA2 WT plasmid or empty vector for 54 h. (D) Immunoblotting of indicated proteins in BT-549 and T-47D PTPN11$^{-/-}$ cells transfected with specified plasmids. (E) Immunoblotting of indicated proteins in BT-549 cells transfected with EPHA2 WT, mutant plasmids, or empty vector for 54 h. (F) Immunoblotting of indicated proteins in BT-549 cells treated with DMSO, PD98059, or LY294002 for 4.5 h after overnight serum starvation.

Figure 9. Negative coupled pathways of SHP-2/ZEB1. (A) Real-time PCR analysis of ZEB1 and SHP-2 in BT-549 cells transfected with vector or ZEB1 plasmids for 24 h. (B) Genomic tracks comparing ZEB1 and control at EPHA2 and PTPN11 promoters. (C) Schematic of SHP-2 promoter fragments; transcription start site ENST00000351677.7 marked as +1. (D) Luciferase assays in BT-549 cells transfected with SHP-2-Luc promoter plasmids, pRL-TK, FLAG-ZEB1, or empty vector for 51 h. (E) Real-time PCR of ZEB1 and EPHA2 in BT-549 cells transfected with vector or ZEB1 plasmids for 24 h. (F) Schematic of EPHA2 promoter fragments; start site ENST00000358432.8 marked as +1. (G) Luciferase assays in BT-549 cells transfected with EPHA2-Luc promoter plasmids, pRL-TK, FLAG-ZEB1, or vector for 52 h. (H, I) Immunoblotting of EPHA2 and SHP-2 in BT-549 cells transfected with vector or SHP-2 plasmid, treated with CHX (H) or CHX plus

MG132 (I) at indicated times. (J, K) Whole-cell proteins from BT-549 cells transfected with FLAG-EPHA2-WT (J) or FLAG-EPHA2-772F (K) incubated with purified SHP-2 at varying concentrations for 30 min at 37°C, followed by immunoblotting for p-EPHA2 (Y772) or phosphorylated FLAG-EPHA2-772F via Phos-tag SDS-PAGE.

Figure 10. Time-dependent multilevel regulation of SHP-2 pathways. (A) Immunoblot of p-SHP-2 (Y542) and total SHP-2 in BT-549 and T-47D cells serum-starved overnight, then stimulated with medium or EGF for 6 h. (B) Quantification of proteins in BT-549 cells stimulated with IL-8, PDGFα, or TGFβ (see S-5B). (C) Quantification of proteins in T-47D cells stimulated with IL-8 or PDGFα (see S-5A). (D) Immunoblot of indicated proteins in BT-549 cells after EGF or IL-6 stimulation for 6 h. (E, F) Quantification of proteins in BT-549 (E) and T-47D (F) cells stimulated with EGF, IL-6, or combined EGF and IL-6 (see S-5C, S-5D).

Supplementary Figure 1. (A) Quantification of sample pairs after SHP-2 immunohistochemical analysis in human breast cancer tissue microarrays (HBreD090CS01, BreD060CS05). (B) Subtypes of the indicated cell lines. (C) cDNA sequence alignment of cell lines via Sanger sequencing. (D) Sanger sequencing of cDNA fragments from T-47D, MDA-MB-231, and BT-549 cells. (E) Representative images of BT-549 cell migration and Matrigel invasion assays after transient transfection with SHP-2 WT (1782) or SHP-2 1794. (F) Spearman correlation between p-SHP-2 (Y580) and p-SHP-2 (Y542).

Supplementary Figure 2. (A) Schematic of ZEB1 promoter fragments with the ENST00000320985.14 start site as +1. (B, C) Luciferase assays in BT-549 (B) and HeLa (C) cells transfected with ZEB1-Luc promoter plasmids, pRL-TK, and expression plasmids for YAP1, JUN, ETS1, or empty vector for 52 h. (D) Immunoblotting of indicated proteins after FLAG-SHP-2 C459S overexpression in BT-549 cells at various time points. (E) Quantification of p-AKT and p-ERK1/2 levels from D. (F) Immunoblotting of indicated proteins after FLAG-SHP-2 overexpression in BT-549 cells for 24 h. (G) SDS-PAGE and Coomassie staining of purified SHP-2 protein (N-terminal SIP tag, C-terminal 6×His tag).

Supplementary Figure 3. (A) ELISA measuring IL-8 levels in indicated cells. (B) Real-time PCR of IL-8 mRNA in indicated cell lines. (C) NC and ZEB1 profiles at TSS ±5 kb regions. (D) Schematic of BP (biological process), CC (cellular component), and MF (molecular function) pathway analyses for ZEB1 target genes. (E, G) Diagrams of IL-6 (E) and IL-8 (G) promoter fragments, with transcription start sites ENST00000258743.10 and ENST00000307407.3 marked as +1. (F) Luciferase assays in HeLa cells transfected with IL-6-Luc promoter plasmids, pRL-TK, and FLAG-ZEB1 or vector for 52 h. (H) Luciferase assays in BT-549 cells transfected with IL-8-Luc promoter plasmids, pRL-TK, and FLAG-ZEB1 or vector for 52 h. (I, J) EMSA of BT-549 nuclear extracts treated with IL-6 (100 ng/mL) and EGF (30 ng/mL) for 12 h, using IR-labeled oligonucleotides with ZEB1 binding sequence on 5% polyacrylamide gel. IR-labeled, cold, and mutant IL-6 binding oligonucleotides are color-coded in (I); additional mutant IL-6 oligonucleotides with further mutations are shown in (J).

Supplementary Figure 4. (A) Schematic of FLAG-SHP-2 WT and its mutants or truncations. (B) Schematic of FLAG-SHP-2 WT and mutants. (C) Whole-cell lysates from BT-549 and T-47D cells

were separated by diagonal gel electrophoresis, blotted, and probed with anti-SHP-2 antibody after denaturation at 37°C for 1 hour. (D) Denaturing non-reducing electrophoresis of SHP-2 in MDA-MB-231, MDA-MB-361, MDA-MB-468, HCC-1954 cells, and purified SHP-2 protein (left: without DTT; right: with DTT; D, dimer; P, polymer; M, monomer). (E) Schematic of FLAG-SHP-2 WT and truncation mutants. (F) Denaturing non-reducing electrophoresis of FLAG in BT-549 PTPN11$^{-/-}$ cells transfected with FLAG-LC, FLAG-LPTPC, FLAG-LNSH2, FLAG-LSH2, FLAG-PTP, or BT-549 WT cells transfected with FLAG-NSH2, FLAG-CSH2, and FLAG-C (left: without DTT; right: with DTT; D, dimer; P, polymer; M, monomer).

Supplementary Figure 5. (A) Immunoblotting of indicated proteins in T-47D cells stimulated with IL-8 or PDGFα at various time points. (B) Immunoblotting of indicated proteins in BT-549 cells stimulated with IL-8, PDGFα, or TGFβ at various time points. (C, D) Immunoblotting of indicated proteins in BT-549 (C) and T-47D (D) cells stimulated with EGF, IL-6, or both at different time points.

Supplementary Figure 6. The black line indicates activation or change; the green line shows reparent interaction, and the dashed green line represents movement direction.

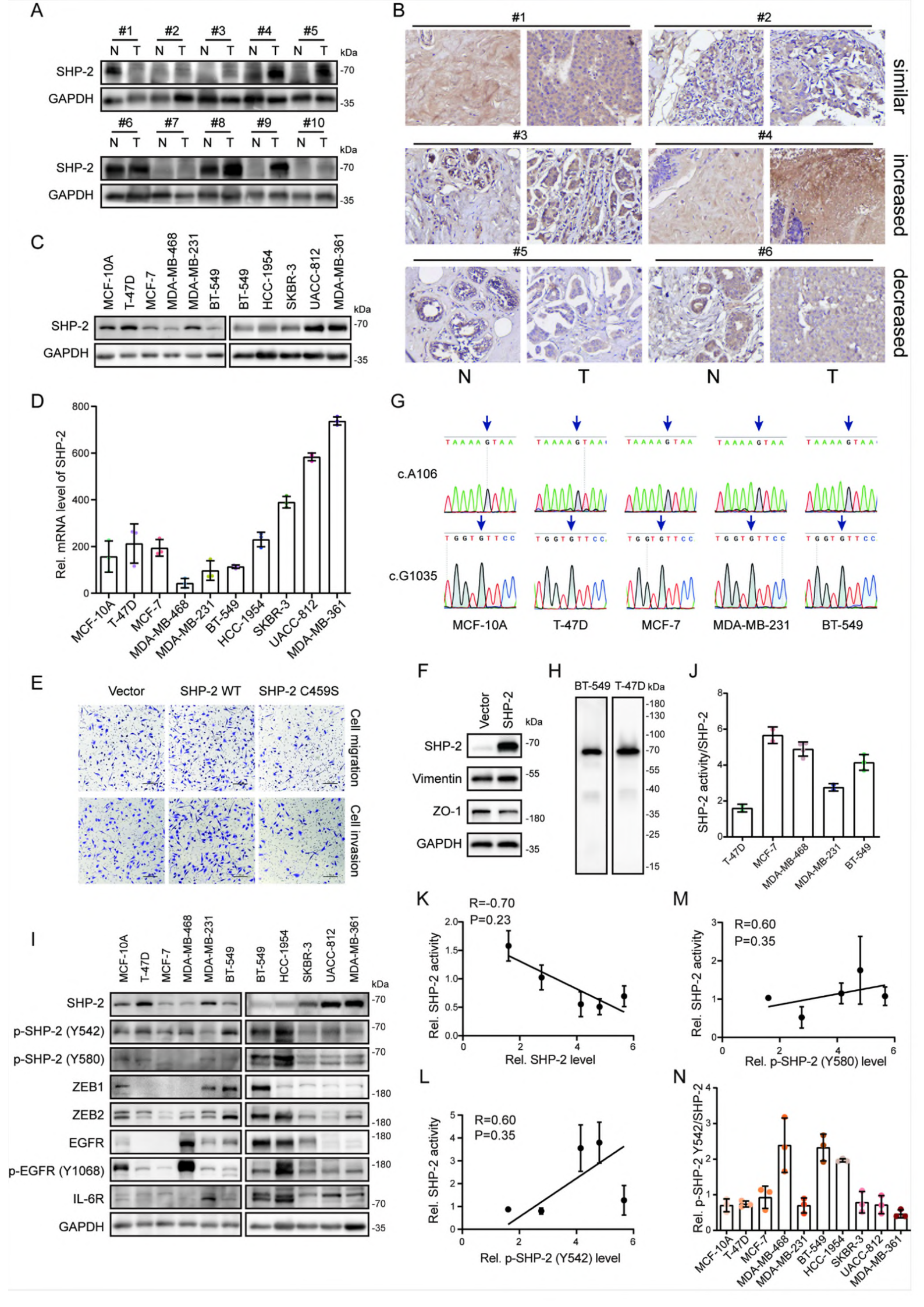
A
#1 #2 #3 #4 #5
N T N T N T N T N T
kDa
SHP-2
GAPDH
-70
-35
#6 #7 #8 #9 #10
B
#1 #2
similar
#3 #4
increased
#5 #6
decreased
N T N T
C
MCF-10A T-47D MCF-7 MDA-MB-468 MDA-MB-231 BT-549 BT-549 HCC-1954 SKBR-3 UACC-812 MDA-MB-361
D
Rel. mRNA level of SHP-2
800
600
400
200
0
E
Vector SHP-2 WT SHP-2 C459S
Cell migration
Cell invasion
F
Vector SHP-2
Vimentin
ZO-1
G
c.A106
c.G1035
MCF-10A T-47D MCF-7 MDA-MB-231 BT-549
H
BT-549 T-47D
J
SHP-2 activity/SHP-2
I
p-SHP-2 (Y542)
p-SHP-2 (Y580)
ZEB1
ZEB2
EGFR
p-EGFR (Y1068)
IL-6R
K
R=-0.70
P=0.23
Rel. SHP-2 activity
Rel. SHP-2 level
L
R=0.60
P=0.35
Rel. p-SHP-2 (Y542) level
M
Rel. p-SHP-2 (Y580) level
N
Rel. p-SHP-2 Y542/SHP-2

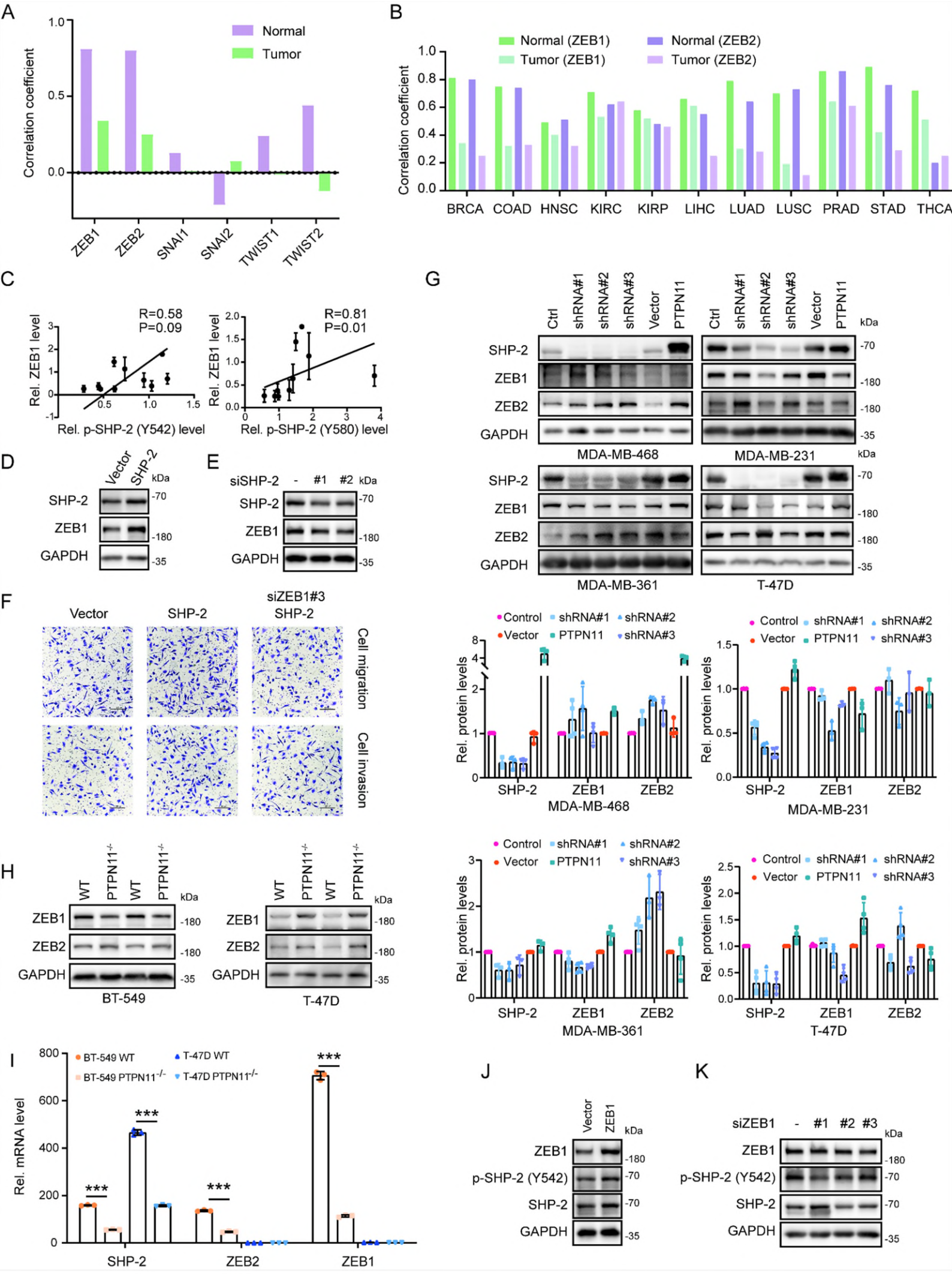
A
Correlation coefficient
Normal
Tumor
ZEB1
ZEB2
SNAI1
SNAI2
TWIST1
TWIST2
B
Normal (ZEB1)
Tumor (ZEB1)
Normal (ZEB2)
Tumor (ZEB2)
BRCA
COAD
HNSC
KIRC
KIRP
LIHC
LUAD
LUSC
PRAD
STAD
THCA
C
R=0.58
P=0.09
Rel. ZEB1 level
Rel. p-SHP-2 (Y542) level
R=0.81
P=0.01
Rel. p-SHP-2 (Y580) level
D
Vector
SHP-2
SHP-2
ZEB1
GAPDH
E
siSHP-2
F
Vector
SHP-2
siZEB1#3 SHP-2
Cell migration
Cell invasion
G
Ctrl
shRNA#1
shRNA#2
shRNA#3
Vector
PTPN11
MDA-MB-468
MDA-MB-231
MDA-MB-361
T-47D
Rel. protein levels
H
WT
PTPN11-/-
BT-549
T-47D
I
BT-549 WT
T-47D WT
BT-549 PTPN11-/-
T-47D PTPN11-/-
Rel. mRNA level
J
ZEB1
K
siZEB1
p-SHP-2 (Y542)

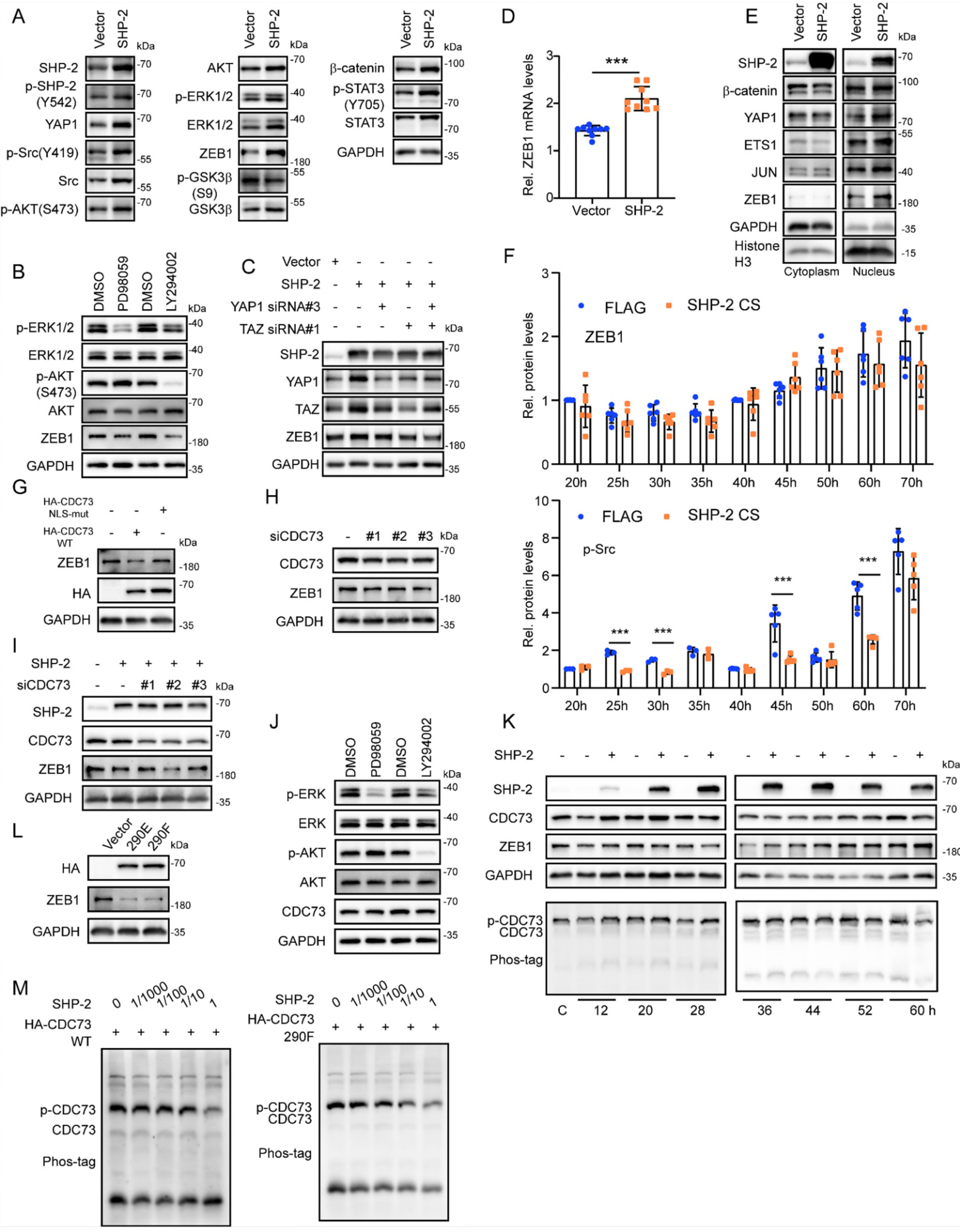
A
Vector
SHP-2
kDa
SHP-2
p-SHP-2 (Y542)
YAP1
p-Src(Y419)
Src
p-AKT(S473)
AKT
p-ERK1/2
ERK1/2
ZEB1
p-GSK3β (S9)
GSK3β
β-catenin
p-STAT3 (Y705)
STAT3
GAPDH
B
DMSO
PD98059
DMSO
LY294002
p-ERK1/2
ERK1/2
p-AKT (S473)
AKT
ZEB1
GAPDH
C
Vector
SHP-2
YAP1 siRNA#3
TAZ siRNA#1
SHP-2
YAP1
TAZ
ZEB1
GAPDH
D
Rel. ZEB1 mRNA levels
***
Vector
SHP-2
E
Vector
SHP-2
SHP-2
β-catenin
YAP1
ETS1
JUN
ZEB1
GAPDH
Histone H3
Cytoplasm
Nucleus
F
FLAG
SHP-2 CS
ZEB1
Rel. protein levels
20h
25h
30h
35h
40h
45h
50h
60h
70h
p-Src
***
G
HA-CDC73 NLS-mut
HA-CDC73 WT
ZEB1
HA
GAPDH
H
siCDC73
#1
#2
#3
CDC73
ZEB1
GAPDH
I
SHP-2
siCDC73
SHP-2
CDC73
ZEB1
GAPDH
J
DMSO
PD98059
DMSO
LY294002
p-ERK
ERK
p-AKT
AKT
CDC73
GAPDH
K
SHP-2
SHP-2
CDC73
ZEB1
GAPDH
p-CDC73
CDC73
Phos-tag
C
12
20
28
36
44
52
60 h
L
Vector
290E
290F
HA
ZEB1
GAPDH
M
SHP-2
0
1/1000
1/100
1/10
1
HA-CDC73 WT
HA-CDC73 290F
p-CDC73
CDC73
Phos-tag

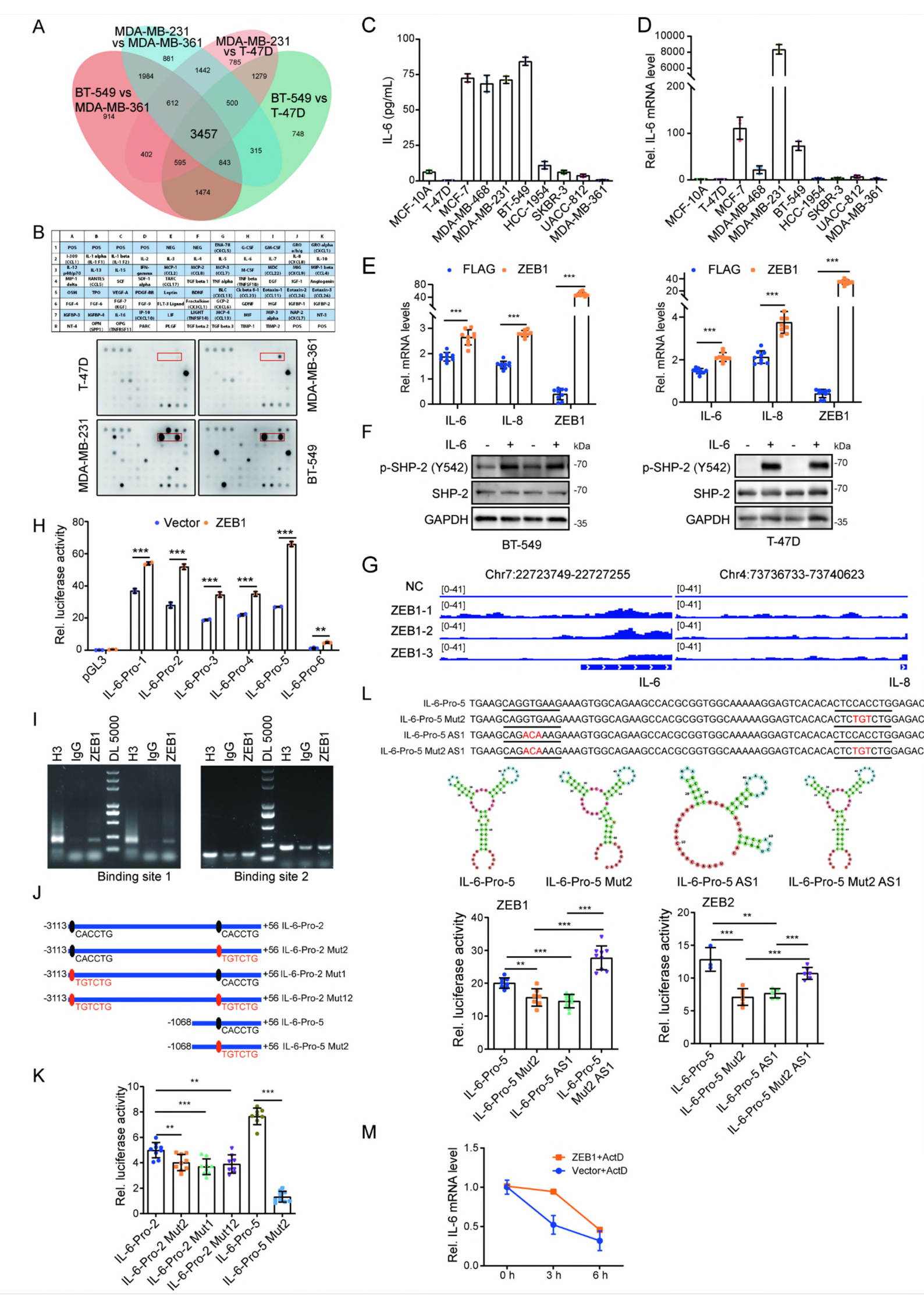
A
MDA-MB-231 vs MDA-MB-361
MDA-MB-231 vs T-47D
BT-549 vs MDA-MB-361
BT-549 vs T-47D
881
785
1984
1442
1279
914
612
500
3457
748
402
315
595
843
1474
B
T-47D
MDA-MB-361
MDA-MB-231
BT-549
C
IL-6 (pg/mL)
MCF-10A
T-47D
MCF-7
MDA-MB-468
MDA-MB-231
BT-549
HCC-1954
SKBR-3
UACC-812
MDA-MB-361
D
Rel. IL-6 mRNA level
E
FLAG
ZEB1
Rel. mRNA levels
IL-6
IL-8
ZEB1
F
IL-6
kDa
p-SHP-2 (Y542)
SHP-2
GAPDH
BT-549
T-47D
G
Chr7:22723749-22727255
Chr4:73736733-73740623
NC
ZEB1-1
ZEB1-2
ZEB1-3
[0-41]
IL-6
IL-8
H
Vector
ZEB1
Rel. luciferase activity
pGL3
IL-6-Pro-1
IL-6-Pro-2
IL-6-Pro-3
IL-6-Pro-4
IL-6-Pro-5
IL-6-Pro-6
I
H3
IgG
ZEB1
DL 5000
Binding site 1
Binding site 2
J
-3113
+56 IL-6-Pro-2
CACCTG
+56 IL-6-Pro-2 Mut2
TGTCTG
+56 IL-6-Pro-2 Mut1
+56 IL-6-Pro-2 Mut12
-1068
+56 IL-6-Pro-5
+56 IL-6-Pro-5 Mut2
K
Rel. luciferase activity
IL-6-Pro-2
IL-6-Pro-2 Mut2
IL-6-Pro-2 Mut1
IL-6-Pro-2 Mut12
IL-6-Pro-5
IL-6-Pro-5 Mut2
L
IL-6-Pro-5 TGAAGCAGGTGAAGAAAGTGGCAGAAGCCACGCGGTGGCAAAAAGGAGTCACACACTCCACCTGGAGAC
IL-6-Pro-5 Mut2 TGAAGCAGGTGAAGAAAGTGGCAGAAGCCACGCGGTGGCAAAAAGGAGTCACACACTCTGTCTGGAGAC
IL-6-Pro-5 AS1 TGAAGCAGACAAGAAAGTGGCAGAAGCCACGCGGTGGCAAAAAGGAGTCACACACTCCACCTGGAGAC
IL-6-Pro-5 Mut2 AS1 TGAAGCAGACAAGAAAGTGGCAGAAGCCACGCGGTGGCAAAAAGGAGTCACACACTCTGTCTGGAGAC
IL-6-Pro-5
IL-6-Pro-5 Mut2
IL-6-Pro-5 AS1
IL-6-Pro-5 Mut2 AS1
ZEB1
ZEB2
M
ZEB1+ActD
Vector+ActD
Rel. IL-6 mRNA level
0 h
3 h
6 h

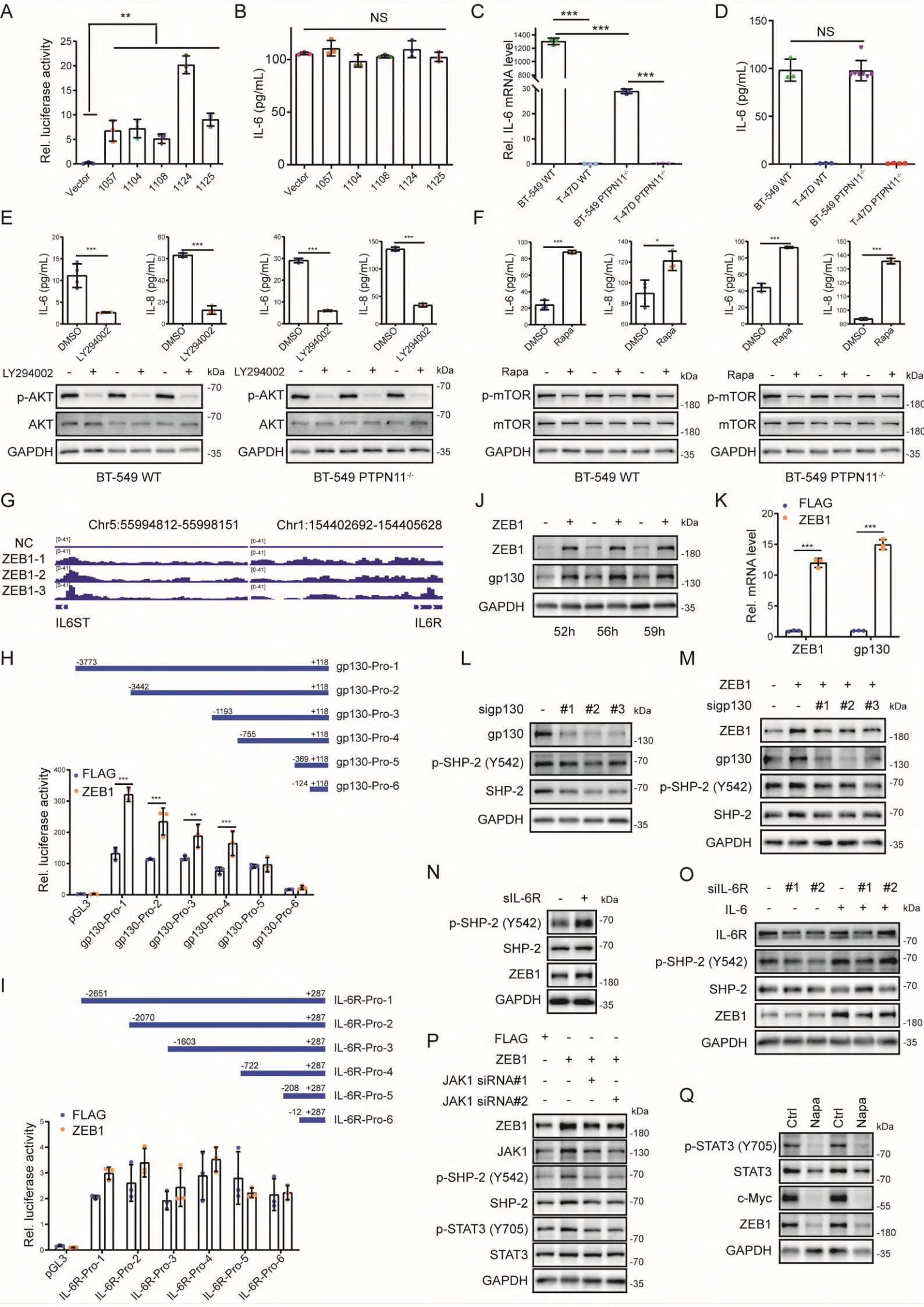
A
Rel. luciferase activity
Vector
1057
1104
1108
1124
1125
B
IL-6 (pg/mL)
NS
C
Rel. IL-6 mRNA level
BT-549 WT
T-47D WT
BT-549 PTPN11-/-
T-47D PTPN11-/-
D
IL-6 (pg/mL)
NS
E
IL-6 (pg/mL)
IL-8 (pg/mL)
DMSO
LY294002
LY294002
kDa
p-AKT
AKT
GAPDH
BT-549 WT
BT-549 PTPN11-/-
F
IL-6 (pg/mL)
IL-8 (pg/mL)
DMSO
Rapa
Rapa
kDa
p-mTOR
mTOR
GAPDH
BT-549 WT
BT-549 PTPN11-/-
G
Chr5:55994812-55998151
Chr1:154402692-154405628
NC
ZEB1-1
ZEB1-2
ZEB1-3
IL6ST
IL6R
J
ZEB1
kDa
ZEB1
gp130
GAPDH
52h
56h
59h
K
FLAG
ZEB1
Rel. mRNA level
ZEB1
gp130
H
gp130-Pro-1
gp130-Pro-2
gp130-Pro-3
gp130-Pro-4
gp130-Pro-5
gp130-Pro-6
FLAG
ZEB1
Rel. luciferase activity
pGL3
gp130-Pro-1
gp130-Pro-2
gp130-Pro-3
gp130-Pro-4
gp130-Pro-5
gp130-Pro-6
L
sigp130
kDa
gp130
p-SHP-2 (Y542)
SHP-2
GAPDH
M
ZEB1
sigp130
kDa
ZEB1
gp130
p-SHP-2 (Y542)
SHP-2
GAPDH
N
sIL-6R
kDa
p-SHP-2 (Y542)
SHP-2
ZEB1
GAPDH
O
siIL-6R
IL-6
kDa
IL-6R
p-SHP-2 (Y542)
SHP-2
ZEB1
GAPDH
I
IL-6R-Pro-1
IL-6R-Pro-2
IL-6R-Pro-3
IL-6R-Pro-4
IL-6R-Pro-5
IL-6R-Pro-6
FLAG
ZEB1
Rel. luciferase activity
pGL3
IL-6R-Pro-1
IL-6R-Pro-2
IL-6R-Pro-3
IL-6R-Pro-4
IL-6R-Pro-5
IL-6R-Pro-6
P
FLAG
ZEB1
JAK1 siRNA#1
JAK1 siRNA#2
kDa
ZEB1
JAK1
p-SHP-2 (Y542)
SHP-2
p-STAT3 (Y705)
STAT3
GAPDH
Q
Ctrl
Napa
Ctrl
Napa
kDa
p-STAT3 (Y705)
STAT3
c-Myc
ZEB1
GAPDH

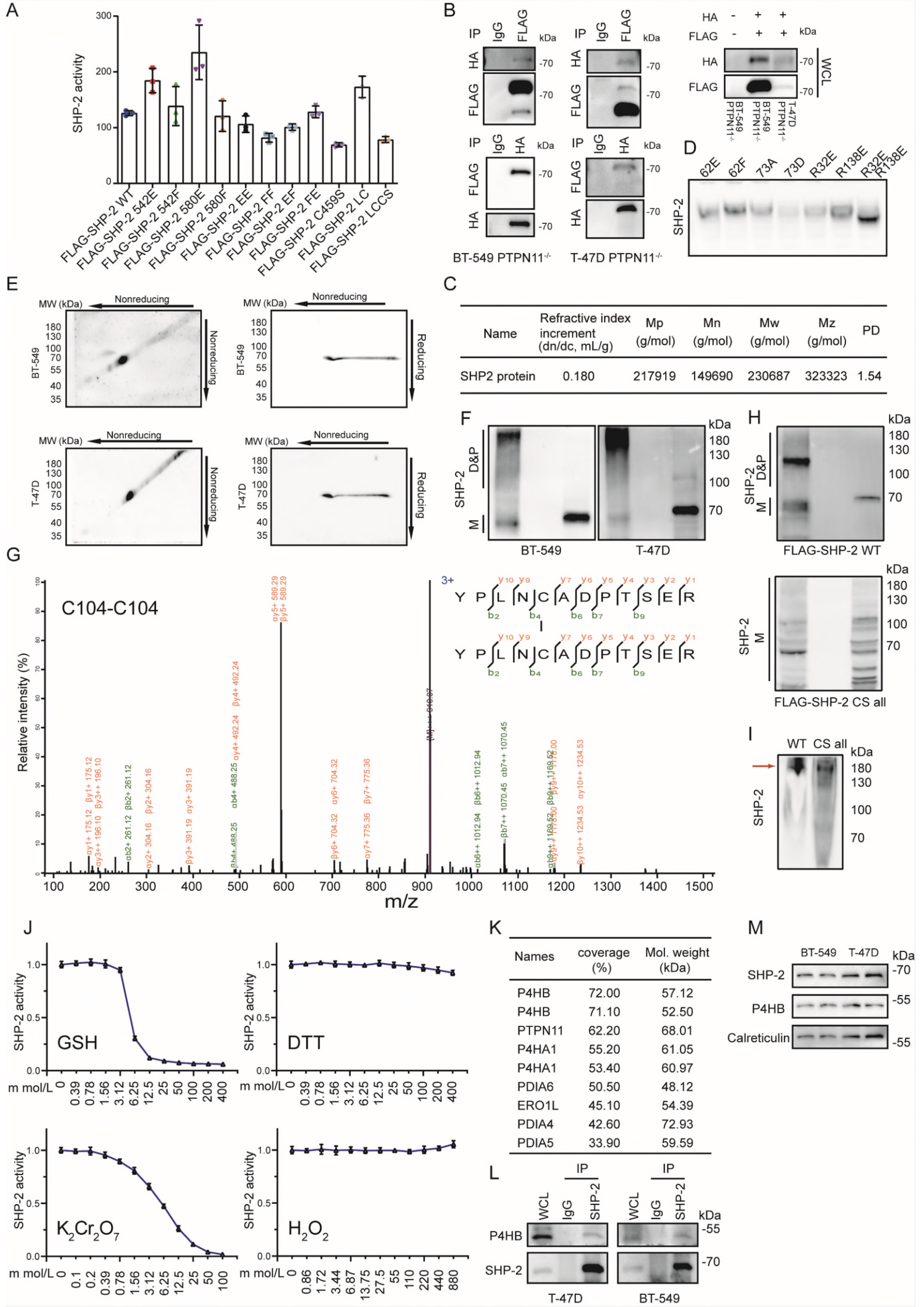
A
SHP-2 activity
FLAG-SHP-2 WT
FLAG-SHP-2 542E
FLAG-SHP-2 542F
FLAG-SHP-2 580E
FLAG-SHP-2 580F
FLAG-SHP-2 EE
FLAG-SHP-2 FF
FLAG-SHP-2 EF
FLAG-SHP-2 FE
FLAG-SHP-2 C459S
FLAG-SHP-2 LC
FLAG-SHP-2 LCCS
B
IP
IgG
FLAG
HA
kDa
WCL
BT-549 PTPN11-/-
T-47D PTPN11-/-
D
62E
62F
73A
73D
R32E
R138E
R32E R138E
SHP-2
E
MW (kDa)
Nonreducing
Reducing
BT-549
T-47D
C
Name
Refractive index increment (dn/dc, mL/g)
Mp (g/mol)
Mn (g/mol)
Mw (g/mol)
Mz (g/mol)
PD
SHP2 protein 0.180 217919 149690 230687 323323 1.54
F
SHP-2
D&P
M
BT-549
T-47D
H
FLAG-SHP-2 WT
G
C104-C104
Relative intensity (%)
m/z
3+
Y P L N C A D P T S E R
FLAG-SHP-2 CS all
I
WT
CS all
J
SHP-2 activity
GSH
DTT
m mol/L
$K_2Cr_2O_7$
H_2O_2
K
Names
coverage (%)
Mol. weight (kDa)
P4HB 72.00 57.12
P4HB 71.10 52.50
PTPN11 62.20 68.01
P4HA1 55.20 61.05
P4HA1 53.40 60.97
PDIA6 50.50 48.12
ERO1L 45.10 54.39
PDIA4 42.60 72.93
PDIA5 33.90 59.59
L
WCL
IgG
SHP-2
P4HB
M
BT-549
T-47D
Calreticulin

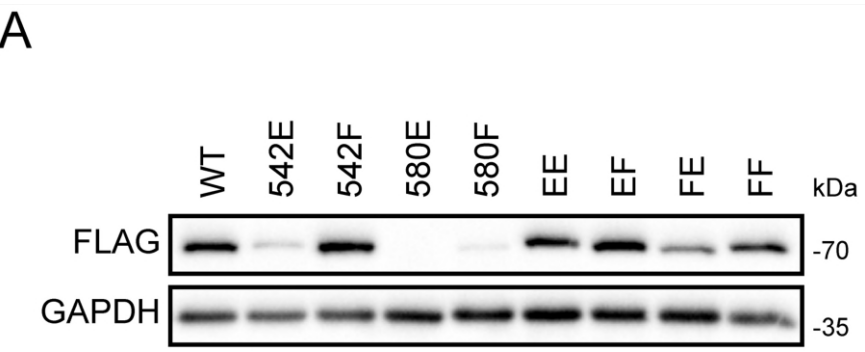
A
WT
542E
542F
580E
580F
EE
EF
FE
FF
kDa
FLAG
GAPDH
-70
-35

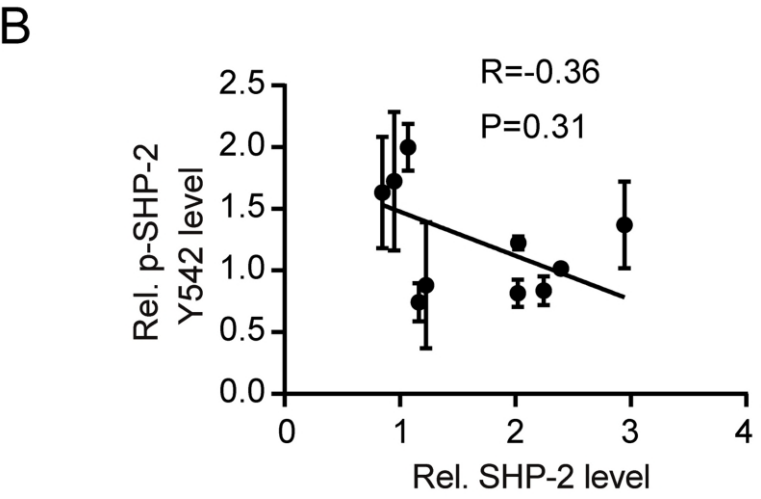
B
R=-0.36
P=0.31
Rel. p-SHP-2 Y542 level
Rel. SHP-2 level
2.5
2.0
1.5
1.0
0.5
0.0
0
1
2
3
4

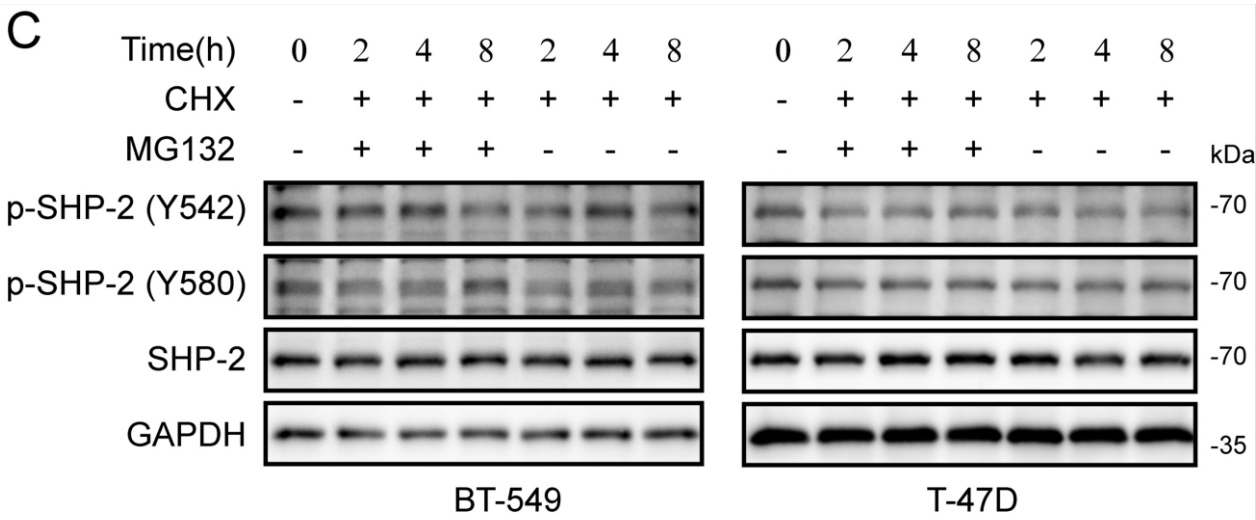
C
Time(h) 0 2 4 8 2 4 8 0 2 4 8 2 4 8
CHX - + + + + + + - + + + + + +
MG132 - + + + - - - - + + + - - -
kDa
p-SHP-2 (Y542)
p-SHP-2 (Y580)
SHP-2
GAPDH
-70
-70
-70
-35
BT-549
T-47D

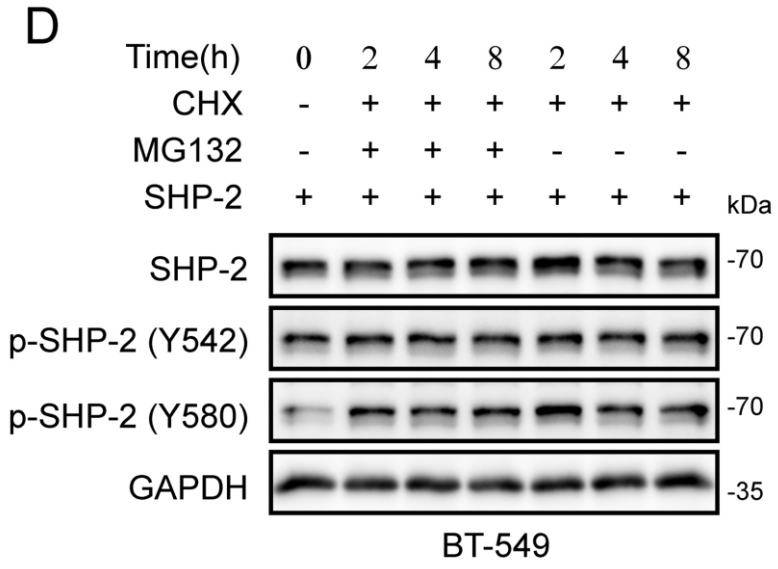
D
Time(h) 0 2 4 8 2 4 8
CHX - + + + + + +
MG132 - + + + - - -
SHP-2 + + + + + + +
kDa
SHP-2
p-SHP-2 (Y542)
p-SHP-2 (Y580)
GAPDH
-70
-70
-70
-35
BT-549

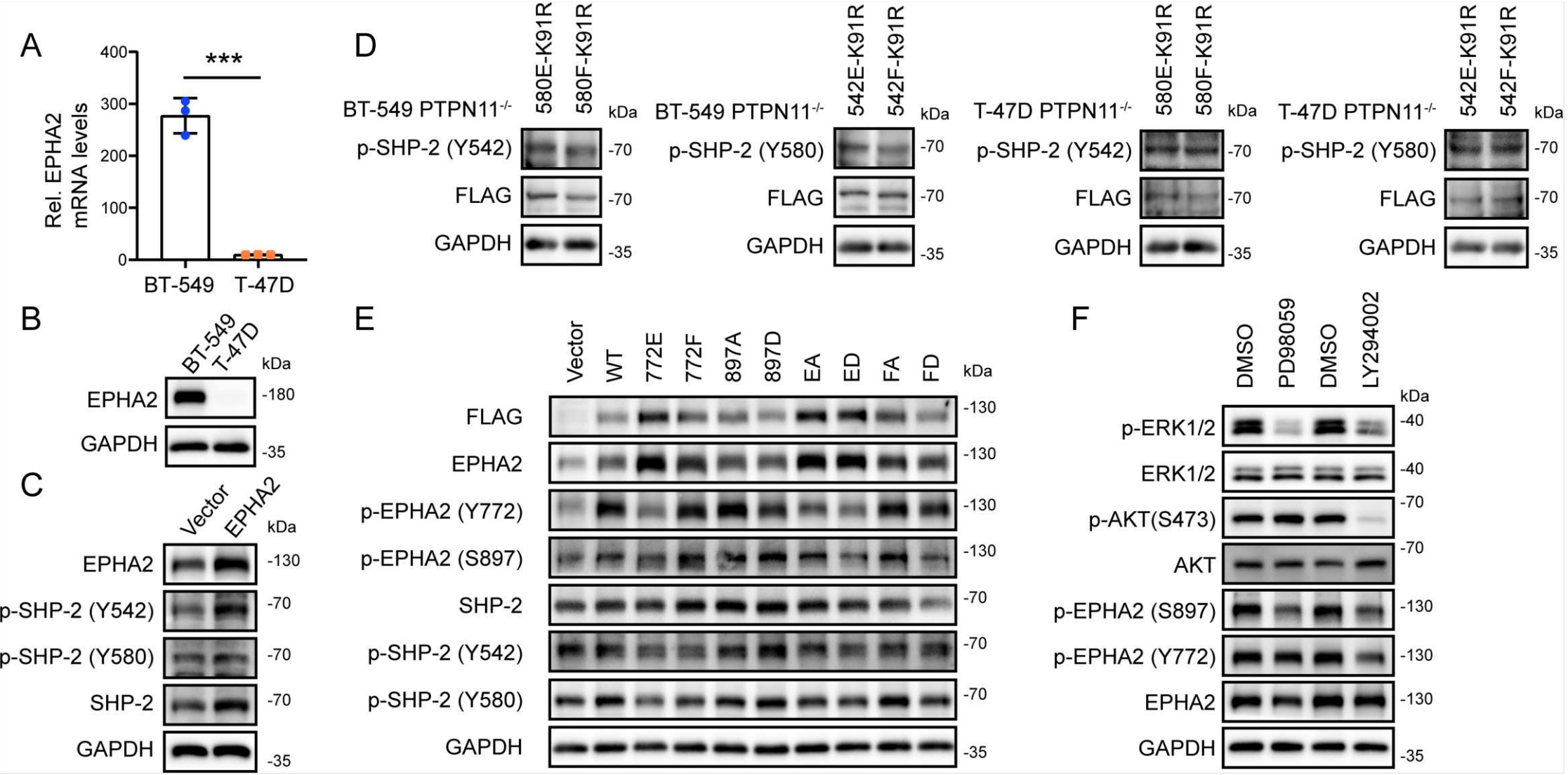
A
Rel. EPHA2 mRNA levels
400
300
200
100
0
***
BT-549
T-47D
B
BT-549
T-47D
kDa
EPHA2
-180
GAPDH
-35
C
Vector
EPHA2
kDa
EPHA2
-130
p-SHP-2 (Y542)
-70
p-SHP-2 (Y580)
-70
SHP-2
-70
GAPDH
-35
D
580E-K91R
580F-K91R
BT-549 PTPN11-/-
kDa
p-SHP-2 (Y542)
-70
FLAG
-70
GAPDH
-35
542E-K91R
542F-K91R
BT-549 PTPN11-/-
kDa
p-SHP-2 (Y580)
-70
FLAG
-70
GAPDH
-35
580E-K91R
580F-K91R
T-47D PTPN11-/-
kDa
p-SHP-2 (Y542)
-70
FLAG
-70
GAPDH
-35
542E-K91R
542F-K91R
T-47D PTPN11-/-
kDa
p-SHP-2 (Y580)
-70
FLAG
-70
GAPDH
-35
E
Vector
WT
772E
772F
897A
897D
EA
ED
FA
FD
kDa
FLAG
-130
EPHA2
-130
p-EPHA2 (Y772)
-130
p-EPHA2 (S897)
-130
SHP-2
-70
p-SHP-2 (Y542)
-70
p-SHP-2 (Y580)
-70
GAPDH
-35
F
DMSO
PD98059
DMSO
LY294002
kDa
p-ERK1/2
-40
ERK1/2
-40
p-AKT(S473)
-70
AKT
-70
p-EPHA2 (S897)
-130
p-EPHA2 (Y772)
-130
EPHA2
-130
GAPDH
-35

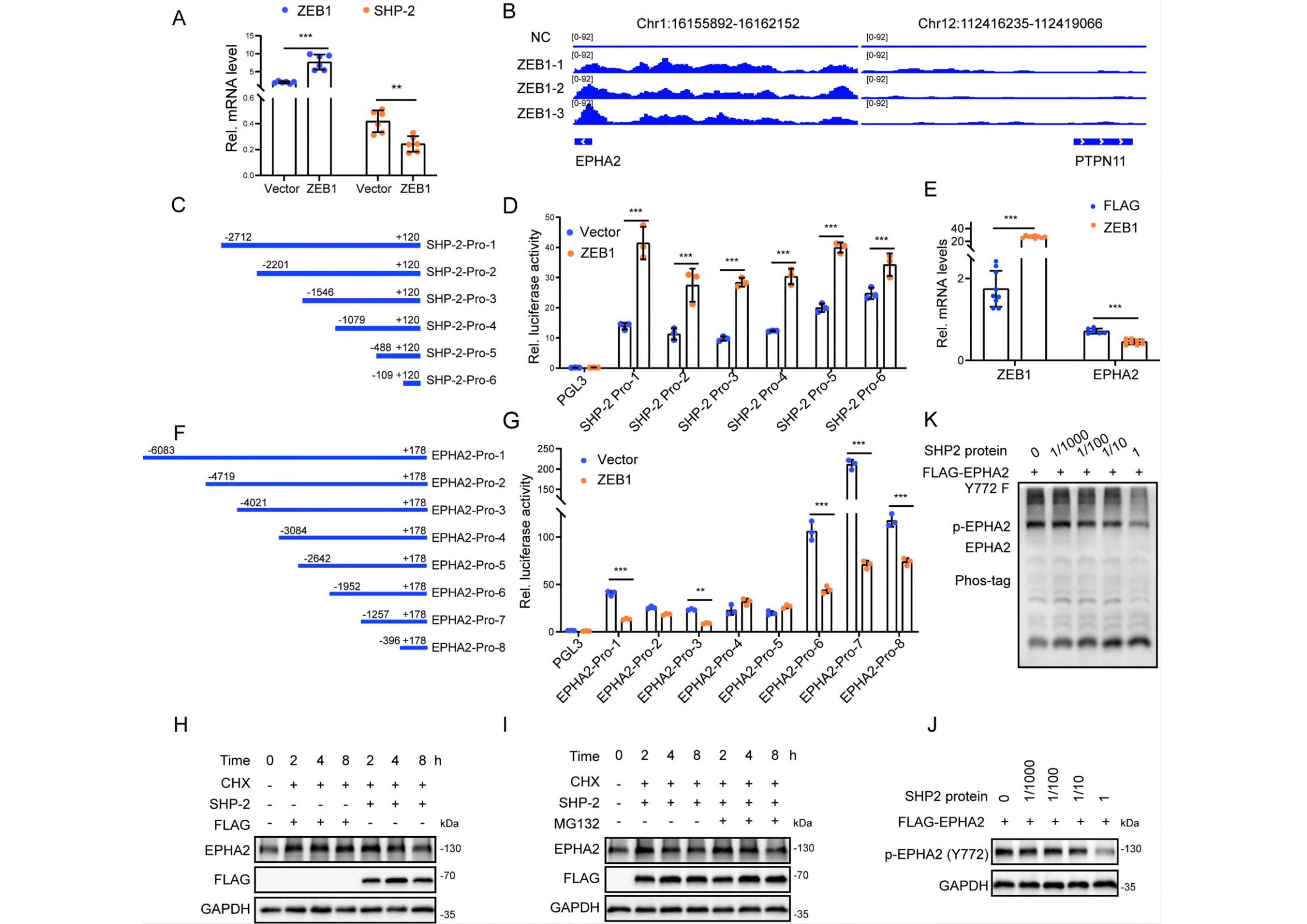
A
ZEB1
SHP-2
Rel. mRNA level
Vector
ZEB1
Vector
ZEB1
B
Chr1:16155892-16162152
Chr12:112416235-112419066
NC
ZEB1-1
ZEB1-2
ZEB1-3
EPHA2
PTPN11
C
SHP-2-Pro-1
SHP-2-Pro-2
SHP-2-Pro-3
SHP-2-Pro-4
SHP-2-Pro-5
SHP-2-Pro-6
D
Vector
ZEB1
Rel. luciferase activity
PGL3
SHP-2 Pro-1
SHP-2 Pro-2
SHP-2 Pro-3
SHP-2 Pro-4
SHP-2 Pro-5
SHP-2 Pro-6
E
FLAG
ZEB1
Rel. mRNA levels
ZEB1
EPHA2
F
EPHA2-Pro-1
EPHA2-Pro-2
EPHA2-Pro-3
EPHA2-Pro-4
EPHA2-Pro-5
EPHA2-Pro-6
EPHA2-Pro-7
EPHA2-Pro-8
G
Vector
ZEB1
Rel. luciferase activity
PGL3
EPHA2-Pro-1
EPHA2-Pro-2
EPHA2-Pro-3
EPHA2-Pro-4
EPHA2-Pro-5
EPHA2-Pro-6
EPHA2-Pro-7
EPHA2-Pro-8
K
SHP2 protein
FLAG-EPHA2
Y772 F
p-EPHA2
EPHA2
Phos-tag
H
Time
CHX
SHP-2
FLAG
EPHA2
FLAG
GAPDH
kDa
I
Time
CHX
SHP-2
MG132
EPHA2
FLAG
GAPDH
kDa
J
SHP2 protein
FLAG-EPHA2
p-EPHA2 (Y772)
GAPDH
kDa

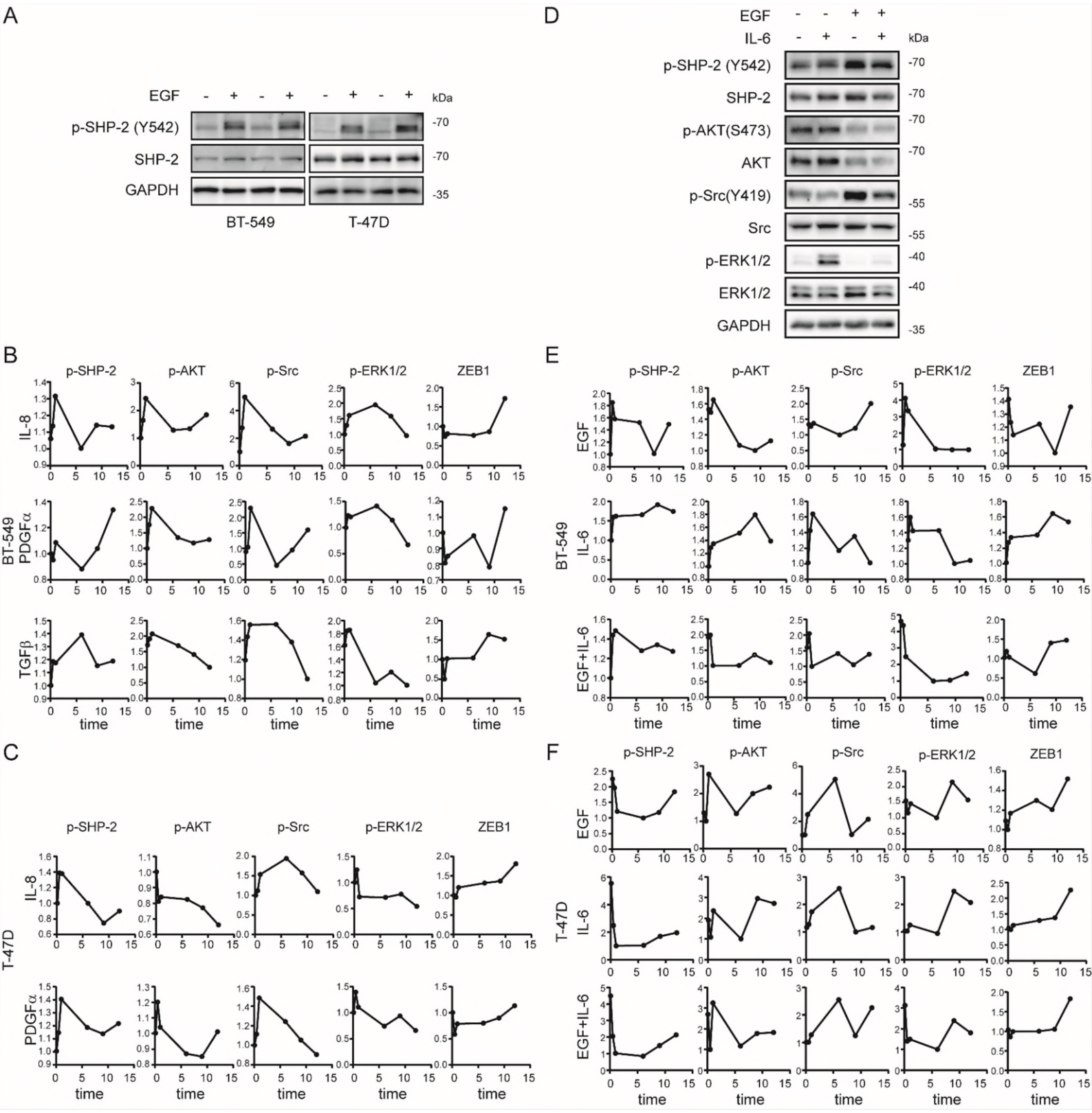
A
EGF - + - + - + - +
kDa
p-SHP-2 (Y542)
SHP-2
GAPDH
-70
-70
-35
BT-549
T-47D
D
EGF - - + +
IL-6 - + - +
kDa
p-SHP-2 (Y542)
SHP-2
p-AKT(S473)
AKT
p-Src(Y419)
Src
p-ERK1/2
ERK1/2
GAPDH
-70
-70
-70
-70
-55
-55
-40
-40
-35
B
p-SHP-2
p-AKT
p-Src
p-ERK1/2
ZEB1
IL-8
BT-549
PDGFα
TGFβ
time
E
p-SHP-2
p-AKT
p-Src
p-ERK1/2
ZEB1
EGF
BT-549
IL-6
EGF+IL-6
time
C
p-SHP-2
p-AKT
p-Src
p-ERK1/2
ZEB1
IL-8
T-47D
PDGFα
time
F
p-SHP-2
p-AKT
p-Src
p-ERK1/2
ZEB1
EGF
T-47D
IL-6
EGF+IL-6
time

Supplementary Files

This is a list of supplementary files associated with this preprint. Click to download.

- Supplementarytable1.docx
- Supplementarytable3.docx
- Supplementarytable2.docx
- SupplementaryFigure3.tif
- SupplementaryFigure4.tif
- SupplementaryFigure6.tif
- SupplementaryFigure5.tif
- SupplementaryFigure2.tif
- SupplementaryFigure1.tif